



Online technique for isotope and mixing ratios of CH₄, N₂O, Xe and mixing ratios of organic trace gases on a single ice core sample

J. Schmitt, B. Seth, M. Bock, and H. Fischer

Climate and Environmental Physics, Physics Institute & Oeschger Centre for Climate Change Research, University of Bern, Bern, Switzerland

Correspondence to: J. Schmitt (schmitt@climate.unibe.ch)

Received: 13 December 2013 – Published in Atmos. Meas. Tech. Discuss.: 3 March 2014

Revised: 3 July 2014 – Accepted: 3 July 2014 – Published: 19 August 2014

Abstract. Firn and polar ice cores enclosing trace gas species offer a unique archive to study changes in the past atmosphere and in terrestrial/marine source regions. Here we present a new online technique for ice core and air samples to measure a suite of isotope ratios and mixing ratios of trace gas species on a single sample. Isotope ratios are determined on methane, nitrous oxide and xenon with reproducibilities for ice core samples of 0.15 ‰ for $\delta^{13}\text{C}\text{-CH}_4$, 0.22 ‰ for $\delta^{15}\text{N}\text{-N}_2\text{O}$, 0.34 ‰ for $\delta^{18}\text{O}\text{-N}_2\text{O}$, and 0.05 ‰ per mass difference for $\delta^{136}\text{Xe}$ for typical concentrations of glacial ice. Mixing ratios are determined on methane, nitrous oxide, xenon, ethane, propane, methyl chloride and dichlorodifluoromethane with reproducibilities of 7 ppb for CH₄, 3 ppb for N₂O, 70 ppt for C₂H₆, 70 ppt for C₃H₈, 20 ppt for CH₃Cl, and 2 ppt for CCl₂F₂. However, the blank contribution for C₂H₆ and C₃H₈ is large in view of the measured values for Antarctic ice samples. The system consists of a vacuum extraction device, a preconcentration unit and a gas chromatograph coupled to an isotope ratio mass spectrometer. CH₄ is combusted to CO₂ prior to detection while we bypass the oven for all other species. The highly automated system uses only ~160 g of ice, equivalent to ~16 mL air, which is less than previous methods. The measurement of this large suite of parameters on a single ice sample is new and key to understanding phase relationships of parameters which are usually not measured together. A multi-parameter data set is also key to understand in situ production processes of organic species in the ice, a critical issue observed in many organic trace gases. Novel is the determination of xenon isotope ratios using doubly charged Xe ions. The attained precision for $\delta^{136}\text{Xe}$ is suitable to correct the isotopic ratios and mixing

ratios for gravitational firn diffusion effects, with the benefit that this information is derived from the same sample. Lastly, anomalies in the Xe mixing ratio, $\delta\text{Xe}/\text{air}$, can be used to detect melt layers.

1 Introduction

The analysis of atmospheric trace gases and their stable isotopic ratios on air archived in ice cores is fundamental to reconstructing and understanding the composition of the atmosphere of the past. Of special interest are studies dealing with the greenhouse gases CO₂, N₂O, and CH₄ due to their radiative forcing. While the long-term temporal changes of their mixing ratios during the past 800 kyr (1 kyr = 1000 years) are broadly known, and in more detail for the last 140 kyr (Loulergue et al., 2008; Lüthi et al., 2008; Schilt et al., 2010), untangling the processes driving these changes remains a challenge. Here, the stable isotopic signatures help to track changes in the atmospheric budget, i.e. to distinguish among sources and sink processes (Sowers et al., 2003; Ferretti et al., 2005; Bock et al., 2010b; Schmitt et al., 2012). For example, N₂O emitted from the ocean is enriched in the heavy isotopologues for both nitrogen and oxygen compared to emissions from terrestrial ecosystems (Rahn and Wahlen, 2000); likewise CH₄ emitted from biomass burning is enriched in the heavy carbon isotope ¹³C compared to microbial CH₄ (Whiticar and Schaefer, 2007). On the other hand, the wide natural variability of a particular source signature often leads to overlaps among sources, and source signatures may change through time (Möller et al., 2013). In addition

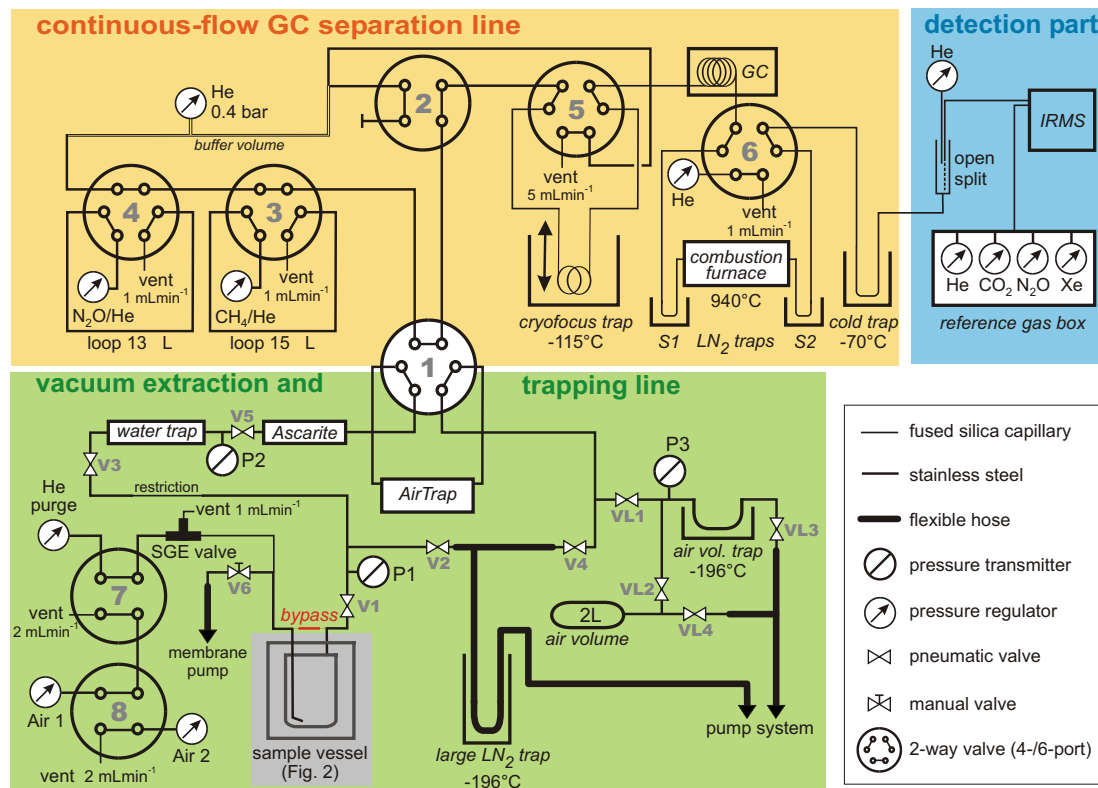


Figure 1. Custom-built analytical set-up comprising the vacuum extraction and trapping line (green), the continuous-flow line with the gas chromatograph (GC) and the combustion furnace (orange), and the detection part (blue). The sample vessel (shaded grey) is sketched in detail in Fig. 2. Note that throughout the paper the 2-way valves (4-/6-port) are referred to as e.g. valve 1, while the Swagelock on/off valves are named e.g. V1.

to these traditional trace gases at ppm (CO_2) or ppb levels (CH_4 and N_2O), CO and atmospheric trace gases at ppt level, like ethane, propane or methyl chloride, are currently being studied in firn (Aydin et al., 2011; Worton et al., 2012) and ice core studies (Saltzman et al., 2009; Wang et al., 2010; Verhulst et al., 2013). Although these ppt-level gases do not significantly influence climate via the greenhouse effect, they act indirectly, e.g. by modifying the lifetime of CH_4 via atmospheric chemistry. Trace gases like ethane, propane, and methyl chloride are predominantly emitted by plants and biomass burning (Pozzer et al., 2010; Xiao et al., 2010). Although not entirely specific for a certain emission type, these trace gases help to constrain possible scenarios in conjunction with other gas species and proxies. For example, methyl chloride shares similarities with CH_4 , as the sources of methyl chloride are also located mostly in tropical regions and the life times of both gases are determined by tropospheric OH as their dominant sink. A challenge for most ppt-level gases (and so far limiting their full usage in ice core research) is the fact that production of these species in the ice itself (in situ production) complicates the atmospheric reconstruction (Aydin et al., 2007; Faïn et al., 2014). Like in the case of CO_2 , where records from Greenland ice

cores have been shown to be obscured by in situ production (Tschumi and Stauffer, 2000), conditions favouring in situ production for N_2O , CH_4 , and trace gases like ethane, propane, and methyl chloride have to be identified.

To analyse isotopes of CH_4 and N_2O on ice core samples, several methods using different extraction techniques have been developed (Sowers et al., 2005; Schaefer and Whiticar, 2007; Behrens et al., 2008; Melton et al., 2011; Sapart et al., 2011; Sperlich et al., 2013; Bock et al., 2014). In contrast, only a few techniques for ice core samples have been established to analyse trace gas species at the ppt level, such as ethane, propane, and methyl chloride (Aydin et al., 2002; Saito et al., 2006; Aydin et al., 2007). Here, we present a new, multi-parameter method to simultaneously measure the mixing ratios and stable isotope ratios of CH_4 and N_2O , the mixing ratios of ethane, propane, and methyl chloride and, additionally, the mixing ratio and isotopic ratio of Xe. This large suite of parameters requires a sample size of only ~ 160 g of ice, which is considerably less than previous methods – a great asset in ice core research, where sample availability is highly limited. Besides sample consumption, deriving all parameters on the same sample is crucial to identify processes within the ice, like in situ production of trace gas

species. For CH₄, these processes have been shown to occur in core sections affected by surface melting (NEEM community members, 2013) or are associated with sharp spikes in aerosol content from biomass burning (Rhodes et al., 2013). In both cases sample size is a critical parameter, and the combined knowledge from many gas species is crucial to identify the underlying processes affecting the archived atmospheric composition of the particular ice core sections.

2 Experimental set-up

Our set-up allows for quantitative extraction and measurement of a large suite of gas species (isotope ratios and/or mixing ratios) in ice and air samples. The set-up shown in Fig. 1 comprises a custom-built online preconcentration system, combining a vacuum melt extraction and a trapping line (Sect. 2.1) including a gas chromatographic separation line (Sect. 2.2). Via an open split this unit is coupled with the detection system, an isotope ratio mass spectrometer (IRMS) described in Sect. 2.3.

2.1 Vacuum extraction and trapping line

The extraction and trapping of the enclosed air of ice samples is carried out under vacuum conditions. The target gases are separated from H₂O, CO₂, and bulk air components (N₂, O₂, Ar) using individual trapping steps.

2.1.1 Sample vessel and melting device

Our sample vessel (~ 350 mL, DN63CF, MCD Vacuum Ltd., UK; Fig. 2) consists of a round-bottom glass part and a stainless steel (SST) flange and holds up to 260 g ice. A capillary (SST, o.d. 1/16", i.d. 0.030") reaching the bottom of the vessel provides the inlet for the reference gas and purge He (Fig. 2). The vessel can be placed into a cooling–melting device – a Plexiglas cylinder that can be automatically cooled to freezing temperatures using a liquid nitrogen (LN₂) pump (Schmitt, 2006; Schmitt et al., 2011) or heated using infrared radiation to melt the ice. An insulating styrofoam lid and fan guarantee a homogeneous temperature distribution throughout the cylinder.

The sample vessel can be bypassed using a 1/16" capillary (SST, i.d. 0.030" named bypass in Fig. 1). It is used for reference gas measurements and air samples and allows tests in which the sample vessel is excluded from the flow path. These gases pass an SGE valve (SGE Analytical Sciences Pty. Ltd., Australia; Fig. 1), which allows us to simulate different sample sizes by changing the time the valve is opened.

2.1.2 Ice melting and trapping processes

The ice is melted using infrared radiation (Fig. 2). Since N₂O and Xe are species with marked water solubility, the preferred extraction technique would be sublimation rather

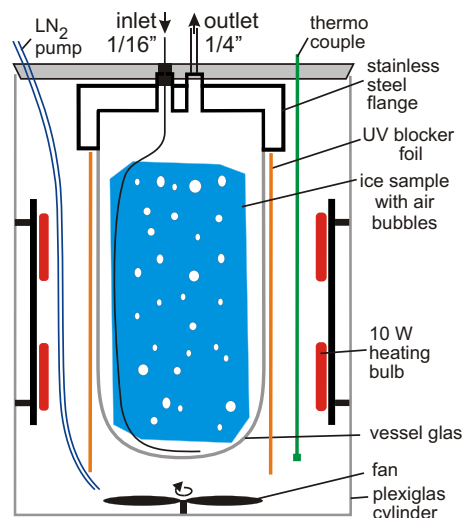


Figure 2. Custom-built vessel holder with sample glass vessel to automatically melt ice samples using infrared light (heating bulbs + UV light blocker foil) or to keep the ice at around -5°C using LN₂ during pumping and procedure blank processing.

than melting. For CO₂ isotope analyses, where sample size (~ 30 g) is much smaller, a sublimation method was recently described (Schmitt et al., 2011). However, the factor of 5 larger sample size needed for isotope analyses of CH₄ and N₂O poses a challenge to using sublimation. While the solubility issue of the melt extraction can be minimised by the melting conditions as discussed below, possible chemical reactions of aerosol-borne impurities due to the presence of a liquid water phase during melting cannot. For gas species, like ethane and methyl chloride but also N₂O, the distinction between chemical reactions happening already in the ice and those occurring during the melting of the ice sample is not trivial. Therefore, results obtained using different extraction techniques, where possible, have to be carefully compared.

As a precaution against possible photochemical reactions of ultraviolet (UV) light with organic material (Vigano et al., 2009), the short wave part of the emitted light, $\sim < 600\text{ nm}$, is absorbed by a UV blocker foil (Schmitt et al., 2011). During the melting process, which lasts ~ 24 min, valves V1, V3, and V5 (diaphragm sealed valves, Swagelok) are open, while the connections to the vacuum pumps (V2, V4, V6, VL1) are closed (Fig. 1). Temperature and melt rates are controlled by regulating the voltage of the lamps and the rate of LN₂ pumped into the Plexiglas cylinder. The released air is dried by freezing out water vapour in the water trap (SST tubing, o.d. 1/4", 8 cm long, i.d. 0.209") held at -80°C . Between the sample vessel and the water trap we installed a restriction (SST, length 3 cm, i.d. 0.030") to adjust the gas flow rates. We set it to optimise pumping efficiency while limiting excessive water from entering the water trap. Low pressure is the main advantage of continuous vacuum extraction compared to melting under He overpressure and is necessary to

extract gases with high solubilities in water at high extraction efficiency (Kawamura et al., 2003; Sperlich et al., 2013). During the melting of the ice sample the total pressure in the vessel (sum of partial pressures of H₂O and air) ranges between 12 mbar at the start and 7 mbar at the end. As the water temperature is close to 0 °C, resulting in a p_{H₂O} of around 6 mbar, the partial pressure of air in the vessel is in the range of only 1 to 6 mbar. For comparison, melt extraction techniques, which melt the ice under He overpressure with closed valves (e.g. Behrens et al., 2008 and Bock et al., 2010a), produce air partial pressures ~ 20 times larger than our values. Equally important to minimise the dissolution of gases into the water during melting is the total pressure as it determines the internal pressure of the rising bubbles in the meltwater.

Sample CO₂ is removed from the air stream by an Ascarite trap (10–35 mesh, Sigma-Aldrich, in 6 cm 1/4" SST tubing, i.d. 0.209"). All other gases, besides He and Ne, are trapped on our AirTrap at –180 °C (SST, 12 cm, o.d. 1/8", i.d. 0.085" filled with activated carbon). During the melting process valves V2, V4, and VL1 remain closed. At the end of the melting process the sample vessel is cooled to +3 °C to keep the water vapour pressure low. Helium is then sent to flow through via the SGE valve into the bottom of the vessel ("purge-He", Fig. 1) and bubbled through the melt water for approximately 14 min at a flow rate of 4 mL min⁻¹ at STP (standard temperature and pressure); VL1 and VL3 are open. We thereby expel the remaining air from the vessel headspace and the tubing towards the AirTrap to achieve quantitative collection. In addition, the He flow strips remaining dissolved gas from the melt water. Simultaneously, the AirTrap is heated to a temperature of –78 °C to keep the gases of interest adsorbed on the activated carbon while 99.99 % of the bulk air components (N₂, O₂, and Ar) are flushed out with the He flow. The extraction and trapping step ends when the AirTrap is switched into the GC line using valve 1 (Fig. 1; 6-port Vici Valco, Vici AG International, Switzerland).

2.1.3 Re-collection of the bulk air

Determining the amount of air corresponding to the trace gas species is necessary in order to calculate atmospheric mixing ratios of these species (additionally, we calculate mixing ratios based on Xe, see Sect. 4.3). The amount of air trapped within the ice sample is also used to calculate the total air content of the ice (Raynaud and Lebel, 1979). To this end, the bulk air leaving the AirTrap at –78 °C is re-collected on the air volume trap at –196 °C (SST tubing, 8 cm, o.d. 1/4", i.d. 0.209", filled with activated carbon; Fig. 1). Afterwards, the trap is isolated (VL1 and VL3 closed), heated to +80 °C, and the released gas is expanded into a thermally insulated 2 L volume by opening VL2. When the pressure reading is stable, pressure and temperature are read out, and mixing ratios of measured gas species are calculated versus

Σ_{air} , i.e. the sum of the bulk air components N₂, O₂ and Ar (see Sect. 4.4).

2.2 GC separation line

The GC line constitutes the continuous-flow part of our set-up (Fig. 1). Helium with 99.9990 % purity (Alphagaz I; Carbagas, Gümligen, Switzerland) is used throughout our system. We further purify this He using a high-capacity gas purifier, an inline gas purifier (both Supelco, Bellefonte, USA), and a custom made purifier trap held at –196 °C (SST, 30 cm, o.d. 1/8", i.d. 0.085", filled with activated carbon). The purifier trap is held at –196 °C during the week and warmed over the weekend for releasing the trapped gases. This purification line provides the He supply for our entire system. The flow of the GC line is controlled by the head pressure of 0.45 bar and the resistance of the GC column. At 30 °C GC temperature the flow is 1.0 mL min⁻¹ and drops to about 0.5 mL min⁻¹ at 220 °C.

When > 99.99 % of the bulk air components have been flushed from the AirTrap, valve 1 is switched from the vacuum line to the GC line, and the AirTrap is heated to 100 °C. The released gases are focused for 22 min on the cryofocus trap (*l* = 90 cm, i.d. 0.32 mm GS-CarbonPlot, Agilent Technologies, USA) held at –115 °C. The design of this cryofocus trap is based on the LN₂-droplet cooled "propeller" trap (Bock et al., 2010a). At this temperature the gases of interest are trapped while residual N₂, O₂ and CO are flushed into the GC.

Upon lifting the cryofocus trap, the gases of interest are released at ~ 80 °C and transferred to the GC column (30 m GS-CarbonPlot). Compounds with a high affinity to the CarbonPlot column at 80 °C, like drill fluid, stay on the cryofocus trap (see Sect. 2.2.1). The GC temperature is held at 30 °C throughout the detection of CH₄, N₂O and Xe. For the organic ppt-level species, temperature is increased in four ramps: 30 to 140 °C in 6 min; 140 to 180 °C in 8 min; 180 to 200 °C in 4 min; 200 to 220 °C in 10 min. The separated species leave the GC column at increasing retention time, as summarised in Table 1. The order of identified species is as follows: CH₄, Kr, CF₄, CO₂, N₂O, ethyne, Xe, ethene, ethane, methyl chloride, propene, propane and dichlorodifluoromethane (CCl₂F₂).

By switching valve 6 during the GC run, only CH₄ and Kr enter the loop containing the combustion furnace, as only CH₄ has to be oxidised to CO₂ prior to detection (Fig. 1). The construction of the combustion furnace is based on Bock et al. (2010a) with a ceramic tube filled with one wire each of Cu, Ni, and Pt (all wires are 0.1 mm o.d., Alfa Aesar, UK) and operated at 940 °C. We oxidise the combustion furnace every morning using the oxygen of the reference air cylinder ("Boulder", see Sect. 3.1.2). Since Kr has almost the same retention time in our system as methane, and doubly charged krypton (⁸⁶Kr²⁺ = *m/z* 43) interferes with the CO₂ measurement producing erroneous results, Kr has to be separated

Table 1. Overview of measured species with their corresponding cup configurations for the seven individual acquisition runs. Time (s) is the elapsed time after the cryofocus trap is lifted, i.e. when a sample is injected onto the GC column. GC (°C) denotes the temperature in the GC when the respective peak is detected in the IRMS. The duration between leaving the GC column and IRMS detection is about 25 s for species eluting at 30 °C and increases to 50 s at 220 °C at the end of the chromatogram due to dropping of the flow rate at higher temperatures. I_{magnet} denotes the magnet current of the focus setting of the mass spectrometer.

No.	Species	Time (s)	GC (°C)	I_{magnet} (mA)	m/z major	m/z minor1	m/z minor2	Detected ions or fragments and remarks
1	Kr	414	30	4000	44	45	46	Kr ⁺ and Kr ²⁺ interference combusted to CO ₂ , delayed by S2 removed by S1 trap and Ascarite
	CH ₄	441	30	4000	44	45	46	
	CO ₂	~ 540	30	4000	44	45	46	
	N ₂ O	586	30	4000	44	45	46	
2	Xe	916	30	4800		66	68	¹³² Xe ²⁺ and ¹³⁶ Xe ²⁺
3	C ₂ H ₄	1020	57	2678	–	–	27	C ₂ H ₃ ⁺ C ₂ H ₃ ⁺
	C ₂ H ₆	1212	118	2678			27	
4	CH ₃ Cl	1592	166	4000	–	–	50	CH ₃ ³⁵ Cl ⁺
5	C ₃ H ₈	1730	177	2678	–	–	29	C ₂ H ₅ ⁺
6	CCl ₂ F ₂	1817	185	4800	–	85	87	C ³⁵ ClF ₂ ⁺ and C ³⁷ ClF ₂ ⁺
7	C ₂ H ₃ Cl ₂ F	> 1900	> 200	4000	–	45	–	C ₂ H ₂ F ⁺

(Schmitt et al., 2013). A first LN₂ trap (“S1”, untreated fused silica capillary) was installed before the combustion furnace to remove background CO₂ while CH₄ and Kr pass the trap. To provide sufficient separation between CH₄-derived CO₂ and Kr, a second LN₂ trap (“S2”, untreated fused silica capillary) is installed behind the outlet of the combustion furnace (Fig. 1). Here, the CH₄-derived CO₂ is trapped at –196 °C while Kr passes and enters the ion source well before the CH₄-derived CO₂ (Schmitt et al., 2013). All other gases bypass the combustion furnace via valve 6 (Fig. 1).

To remove water vapour prior to the mass spectrometric detection, such as water formed from the combustion of methane, the He flow passes a cold trap (30 cm fused silica capillary, i.d. 0.32 mm, –70 °C).

2.2.1 Dealing with drill fluid residues

Deep ice cores are drilled with the help of drill fluids, usually a mixture of hydrocarbons, e.g. kerosene and a densifier. A widely used densifier is HCFC-141b or C₂H₃Cl₂F (Augustin et al., 2007). Problems during the analysis of ice cores caused by traces of drill fluid, which are enclosed in the ice during the drilling process, are widespread and compromise the results of isotopic and trace gas measurements (Aydin et al., 2007; Schmitt et al., 2011; Rubino et al., 2013). During our first ice core measurements we encountered drill fluid contaminated samples, which led to baseline distortions and changes in the retention times. Therefore, a six-port valve was installed, which prevents the drill fluid from entering the GC column (Fig. 1, valve 5). Once the gases of interest have been transferred from the heated cryofocus trap, valve 5 is switched to backflush the trap. To achieve this, the cryofocus trap is heated to 160 °C using an infrared lamp (OSRAM, Augsburg, Germany). While this procedure removes

the largest fraction of drill fluid components, a harmless part still makes its way into the GC and is monitored using its m/z 45 fragment (Table 1).

2.3 Inlet system and mass spectrometer

2.3.1 Inlet system

The GC system is connected to the mass spectrometer via an open split to introduce a constant fraction of sample. The inner diameter and length of the inlet capillary (fused silica, i.d. 100 µm, length 150 cm) controls the flow rate to the ion source (ca. 0.3 mL min^{–1}). In routine operation the vacuum in the source chamber of the mass spectrometer is 2.6×10^{-6} mbar. A reference inlet system controls the injection of pure CO₂ and N₂O gas pulses into the mass spectrometer via SGE valves and a second inlet capillary (reference gas box, Elementar, Hanau, Germany), and a fraction is sucked into the ion source. The pure CO₂ (“Quellkohlenäure”, Messer AG, Switzerland) has $\delta^{13}\text{C}$ and $\delta^{18}\text{O}$ values of -44.300 ± 0.005 ‰ vs. Vienna Pee Dee Belemnite (VPDB) and 30.807 ± 0.067 ‰ vs. Vienna Standard Mean Ocean Water (VSMOW), respectively (dual inlet measurements performed in our division by P. Nyfeler). For the N₂O gas (“N₂O for medical use”, Carbagas, Switzerland) the isotopic composition is unknown and both δ values are set to 0.00 ± 0.00 ‰. In addition to serving as preliminary reference for the sample peaks, the on/off peaks admitted through this reference gas box are used to monitor the performance of the mass spectrometer and to correct for temporal drifts, where appropriate. Besides CO₂ and N₂O, rectangular Xe pulses (1.00 % Xe in He) are injected with our modified reference gas box to provide a reference for the Xe sample peak.

2.3.2 Continuous-flow IRMS

For the continuous-flow analyses we use an IsoPrime IRMS (Elementar, Hanau, Germany). Our IsoPrime is equipped with a universal triple collector plus two additional cups to monitor m/z 28 and 32, named N₂-cup and O₂-cup, respectively; details are described in Schmitt et al. (2013). This cup configuration allows for various source settings to analyse gas species of up to m/z 85 and, coincidentally, isotope analysis of doubly charged Xe isotopes.

The measurement of several gas species on a single sample requires that the IRMS is operated with different source focus parameters and magnet current settings to accommodate the different m/z requirements. For each species or group of species a dedicated set of IRMS source parameters and Ion-Vantage scripts (the IsoPrime control software) is selected, subsequently referred to as a run. To measure all species of a sample, we consecutively start individual runs, each run framing the peaks of the respective gas species (see Fig. 3). Between the individual runs the IRMS source parameters are adjusted, requiring about 30 s to jump from one source setting to the next. Depending on the application, a sample measurement comprises a sequence of up to seven runs (Table 1). Run no. 1, which is the longest run with ca. 5000 s (Fig. 3a), uses the CO₂-N₂O focus setting and our default magnet current of 4000 mA. The detection of Xe and CCl₂F₂ (run 2 and 6) requires that the magnet current is increased to 4800 mA leading to a transient warming of the magnet. To achieve stable peak centre conditions for the next CO₂-N₂O run, the lengths of runs with deviating magnet currents are minimised, and the final run 7 (drill fluid components) again uses the CO₂-N₂O source setting. For runs no. 3–7 we do observe disequilibrium effects on the peak centre positions due to changed magnet current leading to a transient warming/cooling of the magnet. However, as we only measure species concentrations rather than isotopic ratios and use the broad minor2 cup, these changes are not critical. By the start of the next sample measurement, the magnet temperature has reached equilibrium and the IRMS is stable. We usually measure a sequence of runs with a selected number of target species as indicated in Table 1. From each run we obtain individual, mass-specific raw data files, which are processed individually (see Sect. 4).

For the CH₄-N₂O run the CO₂-cup configuration is used, collecting the major isotopologues of CO₂ and N₂O. Molecular nitrogen and oxygen are monitored using the N₂- and O₂-cups. All other species are measured as appropriate ions according to their mass spectra (National Institute of Standards, US: <http://webbook.nist.gov/chemistry>). For example, for both ethene and ethane, m/z 28 is the dominant ion in the mass spectra, but traces of background N₂ interferes at this m/z . Therefore, the less abundant m/z 27 ion is chosen, which allows the measurement of both gases in the same run. Besides these organic trace gas species, we measure the intensities of two Xe isotopes at m/z 66 and 68 reflecting

the doubly charged ions ¹³²Xe²⁺ and ¹³⁶Xe²⁺, respectively, which is a novel application for CF-IRMS (see Fig. 4 and Sect. 4.2). To our knowledge this is the first time doubly charged Xe ions have been used for stable isotope analysis.

3 Analytical procedure

3.1 Sample material and preparation

Our experimental set-up is designed for analysing gas species from air extracted from ice core samples, bottled air samples, and working standard gases.

3.1.1 Ice preparation

The size of the measured ice core sample is ~160 g after about 40 g of ice from the surface is removed with a band saw and a scalpel in a first decontamination step. Possible lab air contamination at or close to the ice surface is removed by sublimation. This second decontamination step is achieved in the sample vessel at vacuum conditions by irradiating the ice sample several times for a few seconds using the heating bulbs. Using the LN₂ pumping system the sample vessel is kept cold at -5 °C throughout the time interval before the ice is melted and is stabilised at +3 °C after all ice is melted to keep pH₂O at ca. 7 mbar.

3.1.2 Air injection

Air samples are run via the bypass (see Sect. 2.1.1 and Fig. 1). Air cylinders need to be at slight overpressure to achieve a flow through the SGE valve of ca. 0.7 mL STP min⁻¹. The amount of air sucked into the vacuum system and trapped on the AirTrap is controlled by timing the opening of the SGE valve. An injection time of 24 min at a constant flow rate of 0.7 mL min⁻¹ is equivalent to ca. 15–17 mL STP or a ~160 g ice sample with entrapped air bubbles. Whole air working standards (externally or in-house calibrated gases) are also run using the bypass. We use two pressurised air cylinders to reference or check the performance of our measurements. The first cylinder CA08289 (“Boulder”), obtained from the National Oceanic and Atmospheric Administration (NOAA) contains air with reduced CH₄ and N₂O mixing ratios of 1508.18 ± 0.17 ppb and 296 ± 11 ppb, respectively. The cylinder was filled in 2008 with ambient background air (~80%), which was diluted with ~20% “ultra-pure air” from Scott-Marrin (D. Kitzis, NOAA, personal communication, 2014). The assigned δ¹³C-CH₄ value for “Boulder” is -47.34 ± 0.02 ‰ (see Table 2). The [N₂O] calibration was carried out by M. Baumgartner ($n = 5$) using a NOAA reference gas (CA03901 315.1 ± 3.2 ppb N₂O). Cross-calibration for δ¹⁵N-N₂O and δ¹⁸O-N₂O via our cylinder “Air Controlé” (see below) is linked to an atmospheric air cylinder from the University of Utrecht (“NAT332”, Sapart et

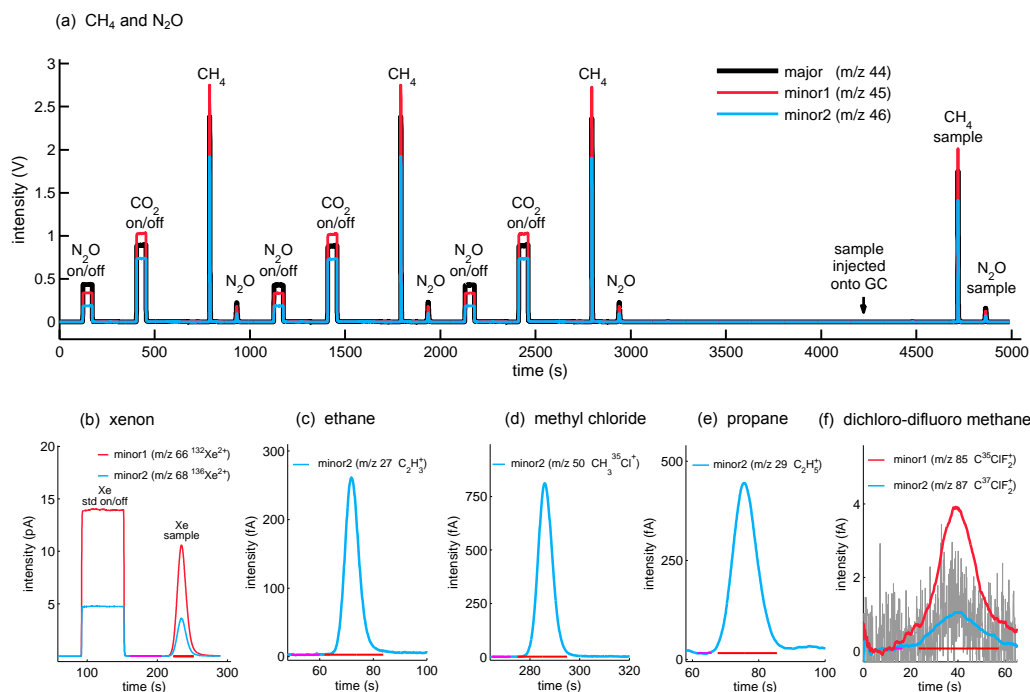


Figure 3. Chromatograms illustrating the sequence of runs and detected gas species at the respective focus settings of the ion source for an Antarctic ice core sample. The order from (a) to (f) follows the increasing retention time starting with CH₄ and ending with CCl₂F₂. (a) CH₄–N₂O-run consisting of rectangular on/off peaks for N₂O and CO₂ admitted by the reference gas box, Gaussian peaks for CH₄ and N₂O injected via valves 3 and 4 (Fig. 1), and sample peaks for CH₄ and N₂O at the end of the run. (b) Xe run consisting of a rectangular on/off Xe peak as reference and the following Xe sample peak. (c–f) show the chromatograms for the organic trace gas species ethane, methyl chloride, propane and dichlorodifluoromethane (CCl₂F₂), respectively, eluting at higher GC temperatures. All chromatograms reflect species concentrations of the ice, except for CCl₂F₂, which serves as an indicator of contamination with modern ambient air. To better visualise the small CCl₂F₂ intensities from the highly amplified minor1 and minor2 cups, the red and blue lines here represent a moving average of 1 s; the minor2 raw signal at 0.1 s resolution is shown as a grey line.

al., 2011). Additionally, with respect to ethane, propane and methyl chloride, our “Boulder” air standard is calibrated on the SIO-05 scale via J-172 by the Swiss Federal Laboratories for Materials Science and Technology (Empa). The mixing ratios of ethane, propane, methyl chloride and dichlorodifluoromethane in “Boulder” are 2673 ± 7 ppt, 1724 ± 5 ppt, 417.3 ± 0.9 ppt and 437.0 ± 0.9 ppt, respectively. Due to the dilution with 20 % “ultra-pure air”, with unknown trace gas composition, it is not clear if the [Xe] and the Xe isotopic composition of “Boulder” is unaffected and still ambient. “Boulder” air is measured on a day-to-day basis together with samples and is used to calibrate samples to the international scales.

The second gas cylinder, CB541659 called “Air Controlé”, contains ambient air and was filled in February 2007 in Basel by Carbagas. The CH₄ and N₂O mixing ratios of 1971 ± 7 ppb and 327 ± 5 ppb, respectively, were determined using conventional gas chromatography (Flückiger et al., 2004). Mixing ratios for ethane, methyl chloride and dichlorodifluoromethane were determined as well at Empa. We assume that our “Air Controlé” cylinder contains [Xe] and Xe isotopes at ambient levels; thus use this cylinder as

our preliminary tie to the atmosphere. Dedicated noble gas measurements on similar fillings of Air Controlé cylinders confirmed this assumption (T. Kellerhals, personal communication, 2014). We measure “Air Controlé” periodically to check long-term consistency of the other cylinders.

Our third gas cylinder is a synthetic gas mixture (“Saphir”, no. 4405, Carbagas, Switzerland) with a [CH₄] of 761 ppb, [N₂O] 315 ppb, [CO₂] 280 ppb and [Xe] 90 ppb. It is measured on a daily basis and mainly serves to detect potential scale drifts in both the CH₄ and N₂O isotope ratios due its contrasting $\delta^{13}\text{C-CH}_4$, $\delta^{15}\text{N-N}_2\text{O}$ and $\delta^{18}\text{O-N}_2\text{O}$ values compared to “Boulder” and “Air Controlé” (see Table 2).

3.2 Measurement scheme

The duration of a measurement varies with the numbers of species measured. The CH₄–N₂O run (measuring m/z 44, 45, 46 for CH₄ and N₂O) takes ca. 80 min. A sequence with all runs (Table 1) takes 140 min. The routine protocol involving an ice sample is as follows: (1) working standard “Boulder” through the *bypass*, (2) working standard “Saphir” over ice, (3) blank over ice, (4) ice sample, treating all

Table 2. List of assigned values for the two reference gas cylinders, their 1σ SD unless otherwise stated, and details on the external calibrations. Values in bold are used to calibrate sample measurements.

Parameter	Unit	“Boulder” CA08289		“Air Controlé” CB541659	
		Value $\pm 1\sigma$ SD	calibration information	Value $\pm 1\sigma$ SD	calibration information
$\delta^{13}\text{C}\text{-CH}_4$	‰ vs. VPDB	-47.34 ± 0.02^a	calibrated at NOAA	–	not externally calibrated
CH_4	ppb	1508.2 ± 0.17^a		1971 ± 7	calibrated with CA03901 ^b
$\delta^{15}\text{N}\text{-N}_2\text{O}$	‰ vs. air N_2	7.55 ± 0.22	cross-referenced to “Air Controlé”	6.94 ± 0.22	measured against “NAT332”, Sapart et al. (2011)
$\delta^{18}\text{O}\text{-N}_2\text{O}$	‰ vs. VSMOW	45.19 ± 0.45		43.45 ± 0.45	
N_2O	ppb	296 ± 11	calibrated with CA03901 ^b	327 ± 5	calibrated with CA03901 ^b
$\delta^{136}\text{Xe}$	‰	0^c	cross-referenced to “Air Controlé”	0 ± 0.06	mean values assigned to 0 as referenced to the present atmosphere
$\delta\text{Xe} / \text{air}$	‰	-8^c		0 ± 22	
C_2H_6	ppt	2673 ± 7	Empa, J-172	2473 ± 2	Empa, J-155
CH_3Cl	ppt	417.3 ± 0.9	Empa, J-172, SIO-2005 scale	445.0 ± 0.7	Empa, J-155, SIO-2005 scale
C_3H_8	ppt	1724 ± 5	Empa, J-172	–	not externally calibrated
CCl_2F_2	ppt	437.0 ± 0.9	Empa, J-172, SIO-2005 scale	528.9 ± 0.2	Empa, J-155, SIO-2005 scale

^a Here the standard error ($n = 18$) is reported instead of 1σ SD. ^b Measured by M. Baumgartner using conventional gas chromatography (Flückiger et al., 2004). ^c Reported are only the mean values as the time series is used for the trend correction.

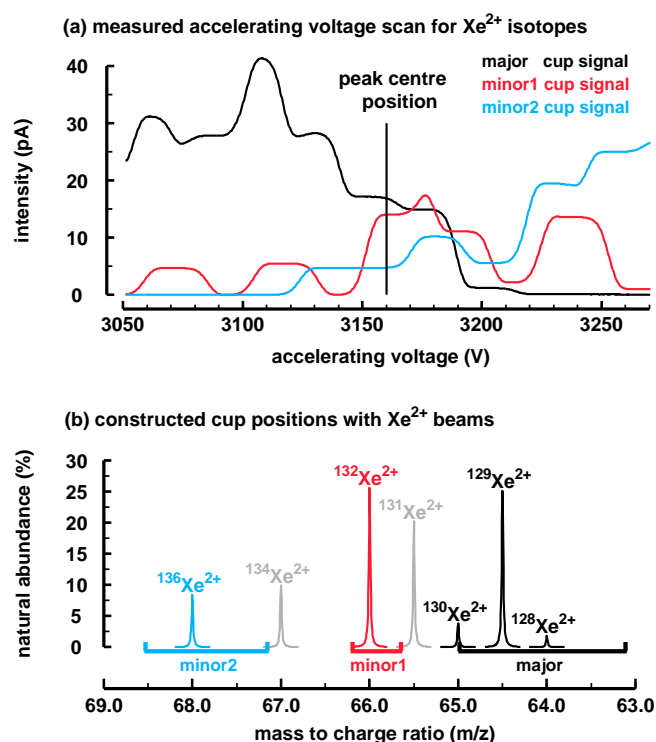


Figure 4. Mass spectrometer focusing to allow for isotope analysis of doubly charged Xe ions. (a) Accelerating voltage scan (note the magnet current was switched from 4000 mA to 4800 mA to allow for the collection of higher m/z ions in the cups) over the region where Xe^{2+} ions hit the Faraday cups. At the selected peak centre position a shared plateau region and the subsequent stable measurement conditions allow for the simultaneous detection of $^{136}\text{Xe}^{2+}$ in minor2 and $^{132}\text{Xe}^{2+}$ in minor1 to calculate isotope ratios spanning 4 m/z units. (b) Constructed Faraday cup configuration and Xe ion beams at peak centre position illustrates that the centre position has to be selected carefully as many Xe^{2+} ions are close to cup edges.

measurements almost identically (Werner and Brand, 2001). Measuring “over ice” means that “Saphir” is injected via the SGE valve into the vessel and pumped towards the *AirTrap*, while the ice sample sits in the cold vessel at -5°C throughout the procedure. The injection takes 24 min, i.e. the same duration as the injection of “Boulder” in the previous bypass measurement or the melting process of the ice in the subsequent measurement. Before the ice sample is melted and measured, we perform a blank measurement over the ice sample (Sect. 3.2.1); this is an additional check whether the vessel is leak tight and provides a first estimate of the samples’ blank contribution. Finally, the ice sample is melted (Sect. 2.1.2), the air extracted and measured.

3.2.1 Blank procedures and extraction efficiency

All analytical steps starting with the gas extraction and the subsequent separation steps can lead to contamination of the analysed gas species. To quantify these “blank contributions” we perform different measurement types. However, none of these blank procedures qualifies to be an identical treatment of the sample procedure. For this, ice with around 10 % gas volume would be required, with the enclosed gas free of the analysed species. As such material is not available, we mimic specific parts of the analysis with individual procedures.

As mentioned above, we routinely run a blank over ice procedure along each ice core sample, called “He over ice sample”. Here, the temperature of the vessel with the ice core sample stays at -5°C throughout the procedure. We process the same amount of He during this blank measurement as for an ice sample measurement and use the same trapping times. All subsequent steps are identical to ice sample measurements. The resulting blank values provide information on the cumulative blank for the entire procedure – except for the melting step, where the extraction vessel is warmed up and water vapour pressure rises. In addition to the blank

resulting from the procedure, around 0.01 mL STP air is collected from the ice core sample itself, as ca. 0.1 g from the ice sample is sublimated at -5°C in the vacuum system.

To explore the effect of melting the ice sample, we process whole procedure blanks termed “gas free ice as sample” using gas-free ice samples. The used ice, which has been produced in a zone melting process, is free of any visible gas inclusions, but could contain traces of gas enclosed in the ice, and thus provides an upper blank estimate.

Blank measurements using the bypass (Fig. 1) are valuable for mimicking air sample or reference gas measurements and allow us to determine the location of leaks and outgassing contributions, e.g. with and without the contribution of the sample vessel. These “He through bypass” measurements follow the same procedure as for “He over ice sample” measurements – except for bypassing the vessel (i.e. a lower blank estimate).

To estimate the extraction efficiency, we run procedure measurements “He through melt water”, where helium is bubbled through the meltwater just after the ice sample measurement. Generally, our vacuum extraction guarantees an extraction efficiency of $> 99.9\%$, e.g. 99.98% for CH_4 and of 99.97% for Xe.

3.2.2 Measurement scheme for CH_4 and N_2O

Previous methods determining both CH_4 and N_2O isotopes on a single ice core sample either used two separate mass spectrometers for CH_4 and N_2O (Sapart et al., 2011) or two individual acquisitions on a single mass spectrometer (Sperlich et al., 2013). To our knowledge we are the first to combine these two isobaric species (CH_4 -derived CO_2 and N_2O) in a single acquisition run. The acquisition of the CH_4 - N_2O run takes 4930 s and starts with three sets of rectangular and Gaussian peak pairs (Fig. 3a). The rectangular on/off peaks comprise pure N_2O and pure CO_2 injected via the reference box (Sect. 2.3.1). While the CO_2 on/off peak is injected, the GC-line status is set to “flow through the oven”, and for the N_2O on/off peak, the valve 6 (Fig. 1) is switched to “bypass the oven” in order to have the same baseline conditions for rectangular and Gaussian peaks. Each pair of on/off peaks is followed by a pair of Gaussian peaks. The first peak is CH_4 (500 ppm CH_4 in He) injected into the GC-line via a $15\ \mu\text{L}$ 1/16" SST loop using valve 3 (Fig. 1). The second is N_2O (250 ppm N_2O in He), injected via a $13\ \mu\text{L}$ loop using valve 4 (Fig. 1). Both loop contents are trapped together on the cryofocus trap and released and transferred to the GC column as described above (Sect. 2.2). The three pairs of rectangular and Gaussian peaks are distributed over two thirds of the chromatogram (Fig. 3a) and allow for drift correction during the acquisition. The vacuum extraction and trapping process occur in parallel to this step (Sect. 2.1). After the gas or ice sample is transferred from the vacuum to the GC line, residual sample N_2 is the first signal to pass the cold cryofocus trap (Sect. 2.3.2). At the end of the acquisition, after the

cryofocus trap is heated, the following peaks are observed according to their respective retention times (see Table 1): the sample Kr peak, the sample CH_4 -derived CO_2 peak, and the sample N_2O peak (Fig. 3a). The separation of Kr and CH_4 is described in detail in Schmitt et al. (2013).

4 Data processing and corrections

The data processing is based on the mass-specific raw data files resulting from the sequence of runs for each measurement (see Sect. 2.3.2). The raw data files produced by Ion-Vantage are processed by our own Matlab (MathWorks) routine, which calculates peak areas and raw isotopic ratios of the species. Isotope ratio calculations are performed for CH_4 , N_2O and Xe using Gaussian sample peaks, which are referenced in a first step to the rectangular on/off peaks for CO_2 , N_2O and Xe, respectively (see Sect. 2.3.1). Especially for the determination of the isotope ratios of N_2O , a robust background correction is crucial for high-precision measurements. As can be seen in Fig. 5, the intensities before the N_2O peak drop due to residual CO_2 , which stems from both the preceding CH_4 -derived CO_2 peak and residual sample CO_2 . A robust, exponential fit of this long-term decay of the major signal can be obtained from the background before the peak, as the signal-to-noise ratio of the major signal is still high $< 0.1\ \text{mV}$ (black dots in Fig. 5). In contrast, fitting a sloping background on the minor1 and minor2 signals (red and blue lines showing a running mean, Fig. 5) is delicate, and the fit becomes more robust with the help of a background interval after the peak. With regard to the integration boundaries, the Matlab script is able to use either start and end slope criteria, fixed time steps left and right from the peak maximum or a fixed percentage of the intensity at peak maximum. The latter approach has resulted in the most reproducible values for N_2O .

In a second step, the individual runs of a species are assembled and analysed to calculate long-term trends and calibration curves. Calculations are carried out e.g. for the blank contribution to the sample peak area using the different types of blank measurements. Further, time-dependent response curves for all species are calculated using the “Boulder” measurements (e.g. for CH_4 , the ratio of the CH_4 peak area vs. the amount of collected air to calculate mixing ratios for samples). For the isotope ratios of CH_4 and N_2O , long-term trends of the reference gases are used to evaluate the scales on which the samples are reported. Also analysed are the isotopic ratios of the additional Gaussian peaks injected for each sample and reference and their relation to the sample and rectangular peaks to identify any drifts in one of the three peak types.

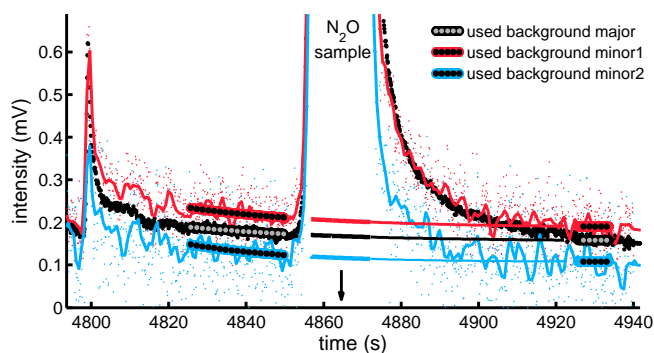


Figure 5. Zoom into the background region of the N_2O sample peak (peak maximum indicated by the arrow). For clarity, the minor1 and minor2 signals are plotted as a 1.5 s moving average to show the faint trends. For the background correction, an exponential fit is calculated using background data before and after the N_2O peak (dotted intervals). The thick solid lines below the N_2O peak indicate the subtracted background signals. Thin lines connect the background below the N_2O peak with the background region after the peak to visually examine the quality of the fitting step.

4.1 Blank estimation and correction

To achieve high-precision mixing ratios and isotopic ratios of trace gases in ice cores, low and quantifiable blank contributions are key aspects of the analytical routine. Firstly, modern mixing ratios and isotopic ratios of the target species can be very different to those found in old ice core air – thus, contamination with modern air has to be minimised. Secondly, outgassing from the extraction vessel, the valve material and the extraction line is of critical concern.

To address the first issue, contamination from modern ambient air, we follow two strategies. First we use the routine blank procedure, “He over ice sample”, before each ice core sample to estimate the blank contribution for the following ice core sample. Secondly, we measure a contamination indicator of modern air directly with each sample as introduced by Aydin et al. (2010). Dichlorodifluoromethane, CCl_2F_2 , is attractive for this purpose, since it currently has the highest mixing ratio of any man-made halocarbon with about 550 ppt, and was absent in preindustrial times (Kaspers et al., 2004). Our detection limit for CCl_2F_2 is 1–2 ppt; thus we can identify modern air contamination to the ice sample to a level of $\sim 0.3\%$ (volume fraction of ambient air relative to the ice core air). An example of a chromatogram for an ice core sample is shown in Fig. 3f, illustrating a CCl_2F_2 signal close to blank level (the ambient air signal intensity would be around 600 fA on minor1). For a typical ice core measurement, the CCl_2F_2 mixing ratio is 3 ± 2 ppt. Taken at face value and using the ~ 550 ppt CCl_2F_2 in ambient air, this value translates into a contribution of $0.5 \pm 0.3\%$ ambient air volume to the air volume of the ice sample. However, this estimate is an upper boundary and relies on the assumption that CCl_2F_2 is co-transported within ambient air

in a macroscopic leak. Generally, the measured CCl_2F_2 and other gas species of modern ambient air can result from various contamination types. First, ambient air can leak or diffuse into the extraction vessel and tubing which are at vacuum conditions. Secondly, modern air can be entrapped in ice core samples from depth ranges shortly below the firn–ice transition, where a small fraction of open porosity is still available for gas exchange. Aydin et al. (2010) dubbed this phenomenon post-coring entrapment of modern air and observed CCl_2F_2 in ice samples that were assumed to be fully closed off (up to 20 m below the estimated firn–ice transition). A few brittle ice samples (600–1000 m depth) from a Greenland ice core (Table 5), however, showed CCl_2F_2 values even exceeding ambient concentrations and may point to high CCl_2F_2 levels during storage in the freezer as described by Aydin et al. (2010). Correspondingly, measuring CCl_2F_2 allows us to identify suspicious measurements, either due to a leak in the extraction system, or from a contaminated ice sample.

Overall, “He over ice sample” measurements give low blank values for CH_4 and N_2O , typically of about 1200 fmol for CH_4 and 550 fmol for N_2O , which is 0.3 % of the average value for Antarctic ice core samples (see Table 3). Assuming that this blank amount (fmol) is added to the ca. 16 mL air of a typical ice core sample, it results in a nominal blank contribution of 1.8 ppb for CH_4 and 0.8 ppb for N_2O (note that the values in Table 3 are given in ppt to allow a common unit for all species). The amount of air typically collected during “He over ice sample” measurements is small with only 0.023 mL which translates to 0.15 % of the amount of air enclosed in our ice samples. A large part of this air likely stems from the ice itself, which is gradually sublimating. The other three blank types show smaller amounts of air (below our detection limit) supporting the view that the blank values are not the result of a leak in the vacuum system. The large blanks observed for the ppt-level species ethane, methyl chloride and propane for all four blank procedure types rather point to an internal source. The most realistic blank types “gas free ice as sample” and “He over ice sample” show blank contributions for methyl chloride in the range of 10–20 % of Antarctic ice samples. Since the methyl chloride blank for “He through bypass” is with 4 % much smaller, the main contribution stems from the extraction vessel. For ethane and propane the blank contributions from the vessel are even higher, especially for the cases where liquid water is present. Clearly, for these two species melt extraction involving a stainless steel flange does not provide acceptable blank values to analyse Antarctic ice core samples.

4.2 Air content

The air content in ice samples is calculated using the read-out at the pressure gauge P3 for the air volume (Fig. 1), the weight of the ice sample, m_{ice} , the internal volume of the air volume, V_{air} , and a calibration factor, $f_{\text{calibration}}$:

Table 3. Results from four procedures to estimate the blank for measured gas species. Values are reported as absolute amounts (fmol), and to bring these values into perspective of the measured ice samples, the values are reported as mixing values (ppt) assuming the measured amounts were added to a typical ice core sample and as percentage of the measured ice core values. * Note that in this table the mixing ratios for all species are given in ppt units, while throughout the paper mixing ratios for CH₄ and N₂O are given in ppb.

type #	“gas free ice as sample” <i>n</i> = 5			“He over ice sample” <i>n</i> = 156			“He through bypass” <i>n</i> = 6			“He through melt water” <i>n</i> = 8		
	(fmol)	(ppt ^a)	(% ^b)	(fmol)	(ppt ^a)	(% ^b)	(fmol)	(ppt ^a)	(% ^b)	(fmol)	(ppt ^a)	(% ^b)
air	< 3 × 10 ⁸	–	< 0.04	1 × 10 ⁹	–	0.15	< 3 × 10 ⁸	–	< 0.04	< 3 × 10 ⁸	–	< 0.04
CH ₄ *	788	1177	0.2	1198	1789	0.3	671	1002	0.2	691	1032	0.2
N ₂ O*	452	675	0.3	554	827	0.3	193	288	0.1	654	977	0.4
¹³⁶ Xe	< 1	< 1.5	< 0.02	6	8.96	0.11	< 1	< 1.5	< 0.02	2	3	0.04
C ₂ H ₆	189	282	80/30	35	52	15/6	30	45	13/5	182	272	77/29
CH ₃ Cl	72	108	21/3	36	54	11/1	15	22	4/1	35	52	10/1
C ₃ H ₈	102	152	73/19	100	149	71/18	36	54	26/7	125	187	89/23
CCl ₂ F ₂	2	2	–	2	3	–	5	7	–	2	2	–

^a would be the increase in the sample mixing ratio if the measured amount of species were added to a typical ice sample with an enclosed air volume of 15 mL STP (6.7×10^{11} fmol). ^b is the percentage of the blank values relative to the values measured for a typical ice core sample. For C₂H₆, CH₃Cl, and C₃H₈, Antarctic values are typically much lower than Greenland values. Therefore, the first values refer to the median of the Antarctic TALDICE samples, and the second values to the Greenland NGRIP samples (see Tables 4 and 5). For the other parameters, only the relation to Antarctica is shown.

$$V = p_{t,corr} \cdot V_{air}/m_{ice} \cdot f_{calibration} \quad (1)$$

To compensate for temperature changes of the expansion volume, the pressure is first corrected for temperature changes, yielding $p_{t,corr}$. As the ice sample slowly sublimates prior to the melting and trapping process, a small fraction of the enclosed air is lost. The total loss is estimated to be around 0.5 % since during the blank over ice processing typically 0.023 mL of air is collected and the corresponding time interval is 30 % of the total sublimation time. Since the internal volume of the air volume and its connections (Fig. 1) is not precisely known (ca. 1900 mL), calibration is necessary to yield accurate values comparable with other groups. To determine the calibration factor $f_{calibration}$, we use our measurements from the Dome C ice core and the accurately calibrated data from the same core (Raynaud et al., 2007). Our data set consists of 59 measurements and the overlapping calibration data comprise 54 points (Fig. 6). The calibration factor $f_{calibration}$ is found by multiplying our data with a varying factor (between 0.98 and 1.02) and selecting the value where the sum of the differences of the time series is at a minimum. We estimate the uncertainty of this calibration procedure, i.e. the accuracy, to be 0.5 mL kg⁻¹ by choosing random subgroups of both time series as input for the calibration. Regarding the achieved precision, Table 5 summarises results from two Antarctic ice cores: (1) vertical pairs of neighbouring samples from the “TALos Dome Ice Core” (TALDICE) and (2) horizontal pairs from the shallow B34 core (75°0.15' S, 00°4.104' E, 2892 m a.s.l., Dronning Maud Land, drilled in the framework of the European Project for Ice Coring in Antarctica (EPICA)). The typical difference for horizontal pairs (B34) is 0.3 mL kg⁻¹ and 0.6 mL kg⁻¹

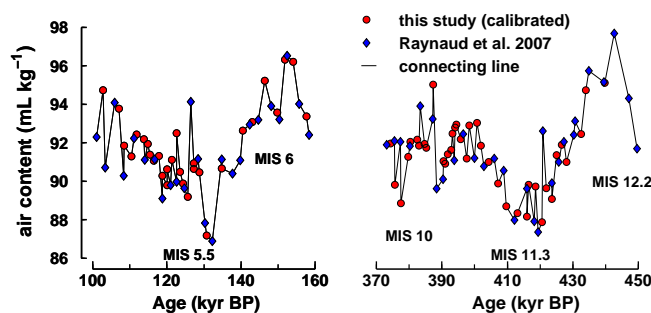


Figure 6. Comparison of our calibrated air content measurements from the Dome C core with published results from the same ice core (Raynaud et al., 2007) plotted on the AICC2012 ice age scale (Bazin et al., 2013; Veres et al., 2013).

for vertical pairs (TALDICE), which is comparable to previous studies (Lipenkov et al., 1995).

4.3 Xenon-based mixing ratios

Atmospheric mixing ratios are usually calculated by referencing the amount (mol) of a species to the amount of total air. However, if an atmospheric gas species is sufficiently constant over the relevant timescale, mixing ratios can be referenced to that parameter as well. In this respect the noble gas Xe can be used, as its past variations on the timescales considered here are smaller than a few per mil, which is lower than our measurement precision (Headly and Severinghaus, 2007). The gravitational fractionation in the firn column can be corrected for with this approach. Typically, the air at the bottom of the firn column is enriched in the heavier gas species by about 0.2 to 0.5 ‰ per mass unit (Craig et al.,

Table 4. Means and 1σ standard deviations of isotope and mixing ratios of CH₄ and N₂O on gases and air extracted from ice samples. n denotes the number of measurements. Note that the isotopic ratios and mixing ratios for CH₄ and N₂O are without gravitational correction, i.e. they represent the composition of the trapped firn air in the ice core. Mixing ratios are not corrected for blank contribution.

Gas measured	n	CO ₂ and CH ₄ -derived CO ₂		N ₂ O		
		$\delta^{13}\text{C}$ (‰)	(ppb)	$\delta^{15}\text{N}$ (‰)	$\delta^{18}\text{O}$ (‰)	(ppb)
pure gases and mixtures in He						
rect on/off CO ₂ , N ₂ O	623	-44.30 ± 0.03		0.72 ± 0.05	37.93 ± 0.09	
gauss _{raw} CH ₄ , N ₂ O	623	-41.80 ± 0.13		1.48 ± 0.22	38.92 ± 0.43	
gauss _{corr} CH ₄ , N ₂ O	623	-41.84 ± 0.08		1.40 ± 0.17	38.82 ± 0.35	
Working gases and air samples						
“Boulder” ^a	320	-47.34 ± 0.12	1508.2	7.55 ± 0.27	45.19 ± 0.58	296
“Saphir”	141	-38.10 ± 0.16	761 ± 10	1.16 ± 0.25	38.12 ± 0.56	316 ± 3
“Air Controlé” ^b	10	-47.79 ± 0.14	1977 ± 19	6.73 ± 0.29	43.39 ± 0.50	323 ± 3
Firn air NEEM	7	-49.49 ± 0.04	1275 ± 21	9.16 ± 0.18	44.91 ± 0.34	289 ± 4
Ice core samples						
B34 (179.12 m)	4	-47.12 ± 0.05	636 ± 9	10.65 ± 0.07	45.92 ± 0.73	260 ± 2
B34 (179.24 m)	4	-47.08 ± 0.05	648 ± 12	10.80 ± 0.23	45.21 ± 0.45	262 ± 4
TALDICE ^c ($\Delta a < 80$ a)	14	-48.56 ± 0.09	556 ± 4	10.88 ± 0.19	45.61 ± 0.39	259 ± 1
TALDICE ^c ($\Delta a < 250$ a)	21	-48.18 ± 0.09	535 ± 6	10.99 ± 0.21	45.75 ± 0.34	254 ± 1
WAIS (170.99 m)	4	-48.03 ± 0.08	710 ± 11	10.30 ± 0.14	45.89 ± 0.46	264 ± 2
NGRIP ^d (134–1461 m)	19	-47.78 ± 0.67	664 ± 45	10.70 ± 0.30	45.53 ± 0.50	265 ± 5

^a Values in bold are the assigned numbers of the isotopic ratios from Table 2, while the reported 1σ values are derived from the measured time series. For the mixing ratios, only the assigned numbers are reported, since here the time series is used to calculate time-dependent response curves. ^b “Air Controlé” values reported here are treated as a sample and calibrated against “Boulder”. Therefore, these values may slightly deviate from the assigned ones in Table 2. ^c For TALDICE the replicate means are shown to put the measured reproducibility into perspective; the reported mean for each parameter is the average of all replicate pairs of the measured time interval (2 kyr to 100 kyr). Note that the reproducibility (\pm value) for TALDICE samples represents the median standard deviation of pairs of “vertical neighbouring replicates”; see Sect. 5.3 for details. ^d The samples from the North Greenland Ice Core Project (NGRIP) are not replicates but single samples covering 10 000 years. Note that a few samples show highly elevated CCl₂F₂ levels (Table 4), but no sample was removed from the calculations as the other parameters seem unrelated to the CCl₂F₂ contamination.

1988; Landais et al., 2006). As the mass difference between e.g. ¹³⁶Xe and CH₄ is 120 mass units, the gravitational fractionation results in ratios which are up to 6 % lower than in the atmosphere. To quantify this gravitational effect, we use the Xe isotope ratio $\delta^{136}\text{Xe}$. We calculate $\delta^{136}\text{Xe}$ from the measured area ratios of ¹³⁶Xe and ¹³²Xe ratio of a sample using the respective ratio of “Air Controlé” as reference and divide by four to report differences per 1 mass unit. The mean reproducibility of ice core replicates for $\delta^{136}\text{Xe}$ is 0.05 ‰ per mass unit. Hence, we can correct each individual ice sample for gravitational enrichment, which is especially advantageous for ice cores with no available gravitational enrichment data (e.g. $\delta^{15}\text{N}$ of N₂). Our precision for the gravitational correction of 0.05 ‰ per mass unit obtained from $\delta^{136}\text{Xe}$ is lower than the results from a dedicated system for $\delta^{15}\text{N}$ (Landais et al., 2006), yet sufficient for our purpose here. Note that using $\delta^{136}\text{Xe}$ to correct for gravitational effects of any gas species in the firn column assumes that the gravitational enrichment of the gases in the firn column is only dependent on the absolute mass difference of two species. Only in the case of sites with large convective zones does this approach produce small biases (Kawamura et al., 2013). In fact,

for Greenland ice cores $\delta^{136}\text{Xe}$ is a better parameter to correct for the gravitational effect than the widely used $\delta^{15}\text{N}_2$, since thermal diffusion effects due to temperature gradients in the firn affect $\delta^{15}\text{N}_2$ more than $\delta^{136}\text{Xe}$ (Severinghaus et al., 2001).

The Xe-based mixing ratio of a sample, hereafter referred to e.g. as $^{Xe}[\text{CH}_4]_{\text{sa raw}}$, is derived from the ratio of the sample’ species’ peak area, $A(\text{species})_{\text{sa}}$, and the area $A(^{136}\text{Xe})_{\text{sa}}$ times the respective ratio of the reference, $A(\text{species})_{\text{ref}}$, and $A(^{136}\text{Xe})_{\text{ref}}$ times the defined mixing ratio of the species of the reference, $[\text{species}]_{\text{ref}}$, following Eq. (2):

$$^{Xe}[\text{species}]_{\text{sa raw}} = A(\text{species})_{\text{sa}} / A(^{136}\text{Xe})_{\text{sa}} / (A(\text{species})_{\text{ref}} / A(^{136}\text{Xe})_{\text{ref}}) \cdot [\text{species}]_{\text{ref}} \quad (2)$$

For each sample measurement we have a reference air measurement from the same day that could be used for a point-wise calculation of the mixing ratio. However, the reproducibility of the ice core replicates is better if a moving average of $A(\text{species})_{\text{ref}} / A(^{136}\text{Xe})_{\text{ref}}$ over several days is used instead, which eliminates the stochastic measurement uncertainty in the daily reference air measurement.

Table 5. Means and 1σ standard deviations of isotope and mixing ratios of trace gases and air content extracted from ice samples. Assigned reference values are in bold. "Boulder" is not listed here since its time series is used to calculate the calibration curves for the parameters. $\delta X_e / \text{air}$ is the anomaly of the atmospheric Xe mixing ratio with respect to the standard in ‰. Mixing ratios are not corrected for blank contribution. Note that CCl_2F_2 is absent in the pre-industrial air, and the reported values for ice samples are contamination. See caption of Table 4 for further information.

Gas measured	<i>n</i>	$\delta^{136}\text{Xe}$ (‰ per mass unit)	$\delta X_e / \text{air}$ (‰)	C_2H_6 (ppt)	CH_3Cl (ppt)	C_3H_8 (ppt)	CCl_2F_2 (ppt)	air content (mL kg ⁻¹)
Working gases and air samples								
"Saphir"	243	0.03 ± 0.06	94 ± 10					–
"Air Controlé"	10	0 ± 0.06	0 ± 22	2414 ± 79	455 ± 17	1763 ± 68	557 ± 11	–
Firn air NEEM	7	0.24 ± 0.06	3 ± 6	2122 ± 22	499 ± 24	612 ± 30	32 ± 1	–
Ice core samples								
B34 (179.12 m)	4	0.43 ± 0.04	2 ± 8	610 ± 156	557 ± 36	404 ± 126	3 ± 2	90.9 ± 0.4
B34 (179.24 m)	4	0.47 ± 0.07	–2 ± 4	551 ± 40	607 ± 25	400 ± 20	3 ± 2	93.7 ± 0.5
TALDICE ($\Delta a < 80$ a)	14	0.34 ± 0.04	6 ± 6	454 ± 77	557 ± 19	316 ± 54	2 ± 2	100.9 ± 0.7
TALDICE ($\Delta a < 250$ a)	24	0.38 ± 0.04	3 ± 8	447 ± 40	568 ± 22	330 ± 29	3 ± 1	101.4 ± 0.6
WAIS (170.99 m)	4	0.30 ± 0.04	–5 ± 14	380 ± 21	916 ± 20	407 ± 75	2 ± 1	111.5 ± 0.4
NGRIP (134–1461 m)	19	0.31 ± 0.04	1 ± 14	945 ± 197	3767 ± 33466	817 ± 179	92 ± 297	88.9 ± 1.9

In the following step the gravitational effect is corrected using the measured $\delta^{136}\text{Xe}$ of the sample, $\delta^{136}\text{Xe}_{\text{sa}}$, times the mass difference between ^{136}Xe and the respective species, Δm :

$$X_e[\text{species}]_{\text{sa}} = (1 - \delta^{136}\text{Xe}_{\text{sa}} \cdot \Delta m / 1000) \cdot X_e[\text{species}]_{\text{sa raw}} \quad (3)$$

For calculating these mixing ratios we use our calibrated "Boulder" cylinder as reference (see Sect. 3.1.3 and Table 2). The thus derived Xe-based mixing ratios compare well with the mixing ratios based on air (see Sect. 4.4 for a comparison of both mixing ratios). Note that the Xe-based mixing ratios cannot be used if the sample contains melt layers, because Xe is more soluble than the main air components (see below).

4.4 Air-based mixing ratios

The calculation of the air-based mixing ratios for a given species is similar to the calculation of the Xe-based mixing ratios. Instead of using Xe, the amount of air, Σair , serves as denominator in the following way:

$$[\text{species}]_{\text{sa raw}} = A(\text{species})_{\text{sa}} / \Sigma \text{air}_{\text{sa}} / (A(\text{species})_{\text{ref}} / \Sigma \text{air}_{\text{ref}}) \cdot [\text{species}]_{\text{ref}} \quad (4)$$

Analogous to the Xe-based version, gravitational fractionation affects the air-based values and is corrected for using Xe isotopes. Here, Δm is the mass difference between the species and the average molecular mass of air (28.8 u):

$$[\text{species}]_{\text{sa}} = (1 - \delta^{136}\text{Xe}_{\text{sa}} \cdot \Delta m / 1000) \cdot [\text{species}]_{\text{sa raw}} \quad (5)$$

Together with the Xe-based mixing ratios from Sect. 4.3, our method allows for the calculation of atmospheric mixing ratios based on two approaches. To keep the figures and tables showing mixing ratios concise, only the air-based results are shown. For the raw mixing ratios, i.e. not corrected for gravitational effects in the firn ($[\text{species}]_{\text{sa raw}}$), the precision of both types of mixing ratios are comparable and the differences are within their combined errors. In contrast, for the CH_4 mixing ratios corrected for gravitational effects, the air-based values are more precise. The typical reproducibility for TALDICE replicates is 5 ppb for the air-based and 7 ppb for the Xe-based value. This is due to the uncertainty of the $\delta^{136}\text{Xe}$ measurement and the large mass difference between CH_4 (16 u) and Xe (136 u), compared to only 16 and 28.8 u in the case of the air-based $[\text{CH}_4]$. The 0.05 ‰ per mass difference uncertainty of the $\delta^{136}\text{Xe}$ measurement and the mass difference of 120 u already lead to an uncertainty of 6 ‰ in the mixing ratio, e.g. 3 ppb for a concentration of 500 ppb.

4.5 Xe air ratio as melt layer proxy

To identify melt layers in polar ice several approaches can be applied. First, melt layers within bubble ice can be identified by visually analysing line scan profiles of the ice core (Abram et al., 2013). This technique works in the bubble ice zone in the absence of clathrates and is very sensitive as millimetre-thick melt layers can be reliably identified. Secondly, total air content measurements provide a proxy for melt layers and can be used to identify melt layers in deep clathrate ice as well (NEEM community members, 2013). The sensitivity of this technique for melt layer detection depends both on the analytical precision and the small-scale variability (mostly annual layering) of the total air content due to changes in the firnification (Hörhold et al., 2012).

Typically, the combined uncertainty of air content measurements is 1 % (Raynaud and Lebel, 1979). To identify melt layers from a reduced air content caused by melting, the “background air content” of unaffected bubble ice has to be established, which is primarily a function of the altitude (Raynaud and Lebel, 1979). The third principle uses the fact that some gases are more water-soluble than other gases, producing characteristic deviations in the mixing ratios of otherwise temporally fairly constant atmospheric gas species. Examples are the noble gases Ar, Kr and Xe (Headly, 2008; NEEM community members, 2013). For the Greenland Dye 3 ice core, Headly (2008) reports $\delta\text{Xe} / \text{Ar}$ ratios for samples with melt layer sections which deviate by 50–100 ‰ from surrounding bubbly ice sections. The air content of these samples is reported to be reduced by 20–50 % compared to bubble ice. Instead of using $\delta\text{Kr} / \text{Ar}$ and $\delta\text{Xe} / \text{Ar}$ ratios, we calculate the parameter $\delta\text{Xe} / \text{air}$ for the same purpose using the gravitationally corrected mixing ratio of ^{136}Xe in air for the sample, $[^{136}\text{Xe}]_{\text{sa}}$, and for the reference, $[^{136}\text{Xe}]_{\text{ref}}$, applying the δ notation as follows:

$$\delta\text{Xe}/\text{air} = ([^{136}\text{Xe}]_{\text{sa}}/[^{136}\text{Xe}]_{\text{ref}} - 1) \cdot 1000. \quad (6)$$

Here, the mixing ratio $[^{136}\text{Xe}]_{\text{ref}}$ is the value for ambient atmospheric air derived from measurements of “Air Controlé”. Note that for this purpose the small changes in the Xe content of the atmosphere due to changes in the ocean temperature can be neglected, as our error of 11 ‰ exceeds the small changes from this process, which amount to only ca. 2 ‰ (Headly, 2008; Ritz et al., 2011).

N_2 and O_2 have lower water solubilities than Ar (Weiss, 1970); thus, the sensitivity of $\delta\text{Xe} / \text{air}$ is higher than $\delta\text{Xe} / \text{Ar}$. The drawback of using air as the denominator of the ratio is that air is a mixture of N_2 , O_2 and Ar, with different water solubilities, yet dominated by the 79 % share of N_2 with a solubility of less than half of that of Ar. Our reproducibility of $\delta\text{Xe} / \text{air}$ for air samples is 10 ‰, and for ice samples without melt layers, typical differences of replicates are 8 ‰ (Table 5). A first feasibility study using Dye 3–88 ice core samples with and without melt layers has shown that our $\delta\text{Xe} / \text{air}$ measurement is sensitive enough to detect melt layers (Fig. 7). With increasing melt fraction (estimated from visual core inspection) and decreasing air content, our $\delta\text{Xe} / \text{air}$ ratio increases. Roughly a 10 ‰ increase in $\delta\text{Xe} / \text{air}$ translates into a decrease of 2.8 mL kg^{-1} in air content. In view of measurement precision only, the air content measurement with a precision of $<1 \text{ mL kg}^{-1}$ is more sensitive to detect individual melt layers than $\delta\text{Xe} / \text{air}$. Yet, detecting melt layers via reduced air content alone requires knowledge of the expected air content of pure bubble ice as the air content at a drill site depends on several parameters (altitude, temperature, impurity content, etc.), which gradually change over time. In contrast, anomalies in noble gas content, e.g. $\delta\text{Xe} / \text{air}$, can be used to detect melt layers without further assumptions and we see its strength especially for

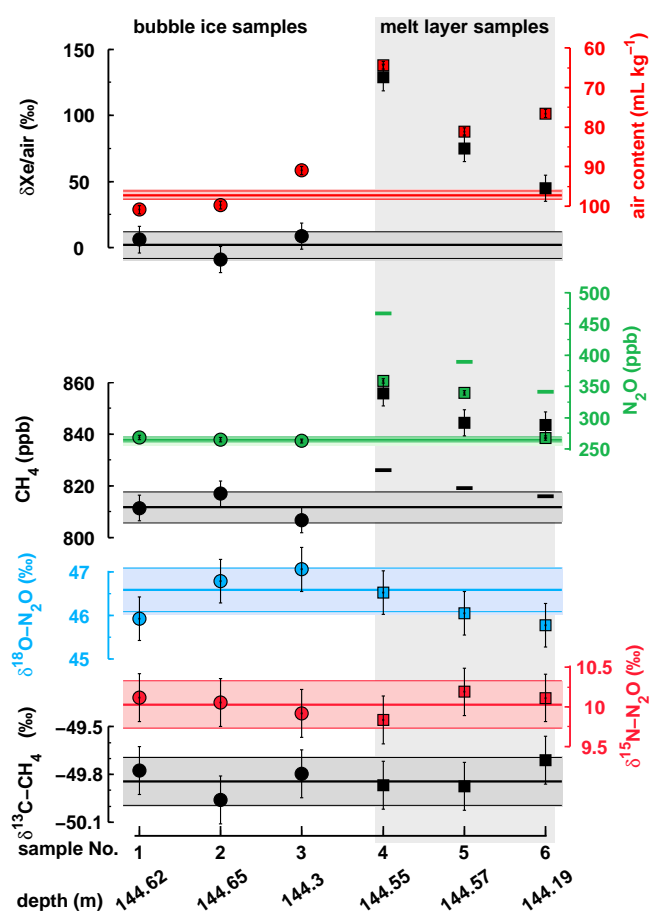


Figure 7. Results of ice core measurements (Dye 3–88, bag 145, depth is given as top of sample) with sections of bubble ice and sections including melt layers. Samples consisting of bubble ice only (no. 1–3) are shown as circles and samples with melt layers (no. 4–6) are shown as squares within grey shading. Note that air content is plotted on an inverse axis. For CH_4 and N_2O , green and black bars, respectively, indicate calculated values in the melt layer samples assuming that both species are affected by equilibrium solubility effects as derived from the $\delta\text{Xe} / \text{air}$ anomaly. Error bars represent the average standard deviation derived from replicate samples (see Table 4). Horizontal shading and lines in the respective species’ colour represent the mean of the bubble ice measurements and 1σ of the typical reproducibility (Tables 4 and 5).

deep ice core sections. In this case, a sample of e.g. 12 cm could cover decades of snow accumulation and one can no longer identify individual melt layers, but our analysis will pick up the melt signal in the sensitive $\delta\text{Xe} / \text{air}$ signal.

Figure 7 shows that CH_4 and especially N_2O are elevated in the melt layers as well. As the solubility of N_2O in water is higher than that of O_2 and N_2 , elevated N_2O values are expected considering solubility effects alone (green and black bars in Fig. 7 showing the expected $[\text{N}_2\text{O}]$ and $[\text{CH}_4]$ values). Surprisingly, both $\delta^{13}\text{C}-\text{CH}_4$ and the N_2O isotopes of the melt layer samples are indistinguishable to the bubble ice

neighbours (Fig. 7). CH₄ in melt layer sections is higher than expected from solubility effects alone (black bars, Fig. 7) which could point to some in situ production in these samples, yet to a much smaller degree than reported previously (NEEM community members, 2013). Since $\delta^{13}\text{C}\text{-CH}_4$ values are unaffected, this points either to an in situ signature close to the atmospheric value, or the fact that CH₄ behaves differently to Xe during melt layer formation. This complicated picture among the different gas species observed from this small feasibility study on melt layers demonstrates that judgements based on a single parameter may lead to biased conclusions. Clearly, a more detailed investigation is necessary to characterise solubility effects and in situ production of CH₄ and N₂O in melt layers.

4.6 Isotope ratios of CH₄ and N₂O

4.6.1 Long-term trends and referencing to international standards

In a first step we reference our isotopic ratios for CH₄ and N₂O on a preliminary scale, which is a pure CO₂ working gas (“Quellkohensäure” see Sect. 2.3.1) in the case of $\delta^{13}\text{C}\text{-CH}_4$ and pure N₂O for $\delta^{15}\text{N}\text{-N}_2\text{O}$ and $\delta^{18}\text{O}\text{-N}_2\text{O}$, both introduced as rectangular on/off peaks. To report our values on an international scale against a reference processed following the identical treatment principle (Werner and Brand, 2001), we use our “Boulder” measurements, which are processed on a daily basis. Similar to the calculation of the mixing ratios, the long-term evolution of the $\delta^{13}\text{C}\text{-CH}_4$, $\delta^{15}\text{N}\text{-N}_2\text{O}$ and $\delta^{18}\text{O}\text{-N}_2\text{O}$ of the “Boulder” measurements are used to reference the samples and to eliminate the stochastic measurement uncertainty in the daily values (see Fig. 8a). For $\delta^{13}\text{C}\text{-CH}_4$, the difference between the assigned value of the “Boulder” air and our preliminary value based on the pure CO₂ working gas (rectangular peaks) is stable over time and amounts to only 0.04 ‰. We thus conclude that the overall isotopic fractionation in our system is very small. For previous methods more significant drifts in the measured $\delta^{13}\text{C}\text{-CH}_4$ values were observed, presumably caused by the combustion unit (e.g. Behrens et al., 2008). In our case a time dependent correction did not further improve precision. For $\delta^{15}\text{N}\text{-N}_2\text{O}$ and $\delta^{18}\text{O}\text{-N}_2\text{O}$ we also observe that the isotopic ratios preliminarily referenced to our pure N₂O working gas do not vary over time, pointing to stable conditions in the overall preconcentration and measurement system. Note, however, that we currently rely on single calibrations only. Samples far away from the isotopic composition of the reference gas composition or a large spread in the samples itself may thus lead to biases due to effects like “isotopic scale compression”. For $\delta^{13}\text{C}\text{-CH}_4$ which shows a large natural range of around 8 ‰ (Möller et al. 2013), round robins are underway and will help deal with this issue. For the N₂O isotopes, the past atmospheric variability in both $\delta^{15}\text{N}\text{-N}_2\text{O}$ and

$\delta^{18}\text{O}\text{-N}_2\text{O}$ is surprisingly small. Thus, any scale effects may have only little influence on the relative differences (Table 4).

4.6.2 Assessing amount effects

Tests regarding a possible dependency of the measured isotope ratios ($\delta^{13}\text{C}\text{-CH}_4$, $\delta^{15}\text{N}\text{-N}_2\text{O}$ and $\delta^{18}\text{O}\text{-N}_2\text{O}$) on peak size were carried out with two contrasting air mixtures, “Boulder” and “Saphir” (see Table 4 for the respective isotopic and mixing ratios). While the isotopic signatures of “Boulder” are close to the range found in ice samples, the artificial “Saphir” mixture has strongly deviating $\delta^{13}\text{C}\text{-CH}_4$, $\delta^{15}\text{N}\text{-N}_2\text{O}$ and $\delta^{18}\text{O}\text{-N}_2\text{O}$, which is ideal to check the system performance at strongly deviating isotope ratios. As mentioned above (Sect. 2.1.1), we simulate different sample sizes by timing the opening of the SGE valve while keeping the flow rate to the vessel constant. To cover the peak size range equivalent from ca. 360 ppb CH₄ to ca. 1500 ppb, injection time for “Boulder” varies between 335 s and 1435 s. Since the isotopic signatures are so different between “Boulder” and “Saphir”, anomalies are calculated to plot the results of both gases in one graph (Fig. 8b and c). In general, no signal dependency on the respective peak size is observed for $\delta^{13}\text{C}\text{-CH}_4$ and $\delta^{18}\text{O}\text{-N}_2\text{O}$. For $\delta^{15}\text{N}\text{-N}_2\text{O}$ there is a small deviation towards lighter values for smaller sample sizes. Figure 8 shows that for $\delta^{13}\text{C}$, precision is almost independent of sample size, while for $\delta^{15}\text{N}\text{-N}_2\text{O}$ and $\delta^{18}\text{O}\text{-N}_2\text{O}$, precision is lower for the smallest peak size, which is, however, far outside the sample range indicated by the arrows.

5 System performance and reproducibility

In the following section we will discuss the precision of the overall system. We will concentrate in this discussion on the isotopic ratios of CH₄ and N₂O. The precision of the ppt-level concentration measurements is listed in Table 5 and only briefly discussed below.

5.1 Pure gases

In the following we discuss the measurement precision of the different components in a sequential way starting with the isotope ratio mass spectrometer, the continuous-flow GC part, and finally the performance of the whole procedure. We use pure gases (CO₂ and N₂O) admitted via the reference gas box, CH₄ and N₂O mixtures in He injected onto the cryofocus, and whole air and ice core samples, respectively. Regarding the IRMS part only, the precisions of the three CO₂ and N₂O on/off peaks injected in each run (1 σ standard deviation of the three values after correcting for temporal drift using a linear fit) are 0.03 ‰, 0.05 ‰ and 0.09 ‰ for $\delta^{13}\text{C}$, $\delta^{15}\text{N}$ and $\delta^{18}\text{O}$ respectively (Table 4, pure gases). For the Gaussian CH₄ and N₂O peaks we achieve precisions of 0.13 ‰, 0.22 ‰, and 0.43 ‰ for $\delta^{13}\text{C}$, $\delta^{15}\text{N}$, and $\delta^{18}\text{O}$ respectively. If the Gaussian peaks are corrected for

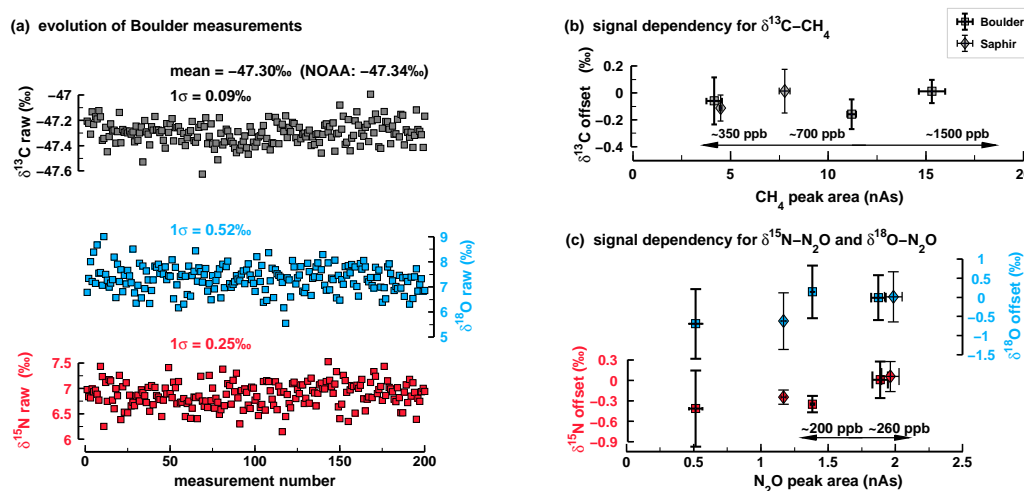


Figure 8. System performance of reference air measurements. (a) Long-term evolution of the measured raw values for the isotopic signatures ($\delta^{13}\text{C}$, $\delta^{15}\text{N}$, $\delta^{18}\text{O}$) of “Boulder” air referenced against pure CO_2 and N_2O on/off peaks spanning a period of 1 year. Effect of sample size and signal intensity on the measured isotope ratios (b) for $\delta^{13}\text{C}$ - CH_4 and (c) for $\delta^{18}\text{O}$ - N_2O and $\delta^{15}\text{N}$ - N_2O . Within the range covered by ice core and ambient air samples, all three isotope ratios are independent of the signal intensity.

the observed linear trend of the on/off peaks, precision improves slightly (Table 4, $\text{gauss}_{\text{raw}}$ and $\text{gauss}_{\text{corr}}$). The good precisions of these Gaussian peaks show that both CO_2 and N_2O peaks can be measured within a run (see Fig. 3 for the injection scheme) without producing significant memory effects. This allows for the measurement of isotopic ratios of different isobaric species within a run, while previous studies measuring CH_4 and N_2O on a single sample either reserved a specific IRMS for each species (Sapart et al., 2011) or held one species until the IRMS was preconditioned for the second species (Sperlich et al., 2013). Currently, the CH_4 and N_2O Gaussian peaks within each chromatogram serve only to monitor the system performance and for troubleshooting. The reference basis for the CH_4 and N_2O sample peaks are the CO_2 and N_2O on/off peaks. When we tested use of the Gaussian peaks to correct sample peaks for any variable fractionation process in the GC part or the combustion oven, reproducibility of samples did not improve.

5.2 Whole air

For estimating the overall precision of our system we calculate the 1σ standard deviation of our daily “Boulder” and “Saphir” measurements. For “Boulder”, we obtain standard deviations of 0.12‰ , 0.27‰ and 0.58‰ for $\delta^{13}\text{C}$ - CH_4 , $\delta^{15}\text{N}$ - N_2O and $\delta^{18}\text{O}$ - N_2O , respectively (Table 3). A similar precision for these parameters is obtained for “Saphir”, which is injected into the cold sample vessel containing the ice sample. As shown for our He over ice measurements, a small fraction of the ice sample sublimates during the “over ice” procedure; thus air is released from the ice sample and “contaminates” the “Saphir” sample. Based on our He over ice blanks, the released amount of ice core air

is 0.023 mL . With a “Saphir” sample volume of 13 mL , this translates to a volumetric contribution of 0.18% . While the CH_4 and N_2O mixing ratios of “Saphir” are close to the range of ice core samples, the isotopic ratios deviate considerably (Table 4). Yet the small contribution of ice core air does not significantly affect the isotopic signatures of CH_4 or N_2O . In addition, two natural whole-air samples have been measured to quantify the reproducibility: “Air Controlé” and firm air from NEEM (Table 4).

5.3 Ice core samples and replicates

Performance values derived from working standards and air samples allow a first approximation of the system performance due to identical treatment, yet determining the reproducibility on real ice samples is nevertheless necessary. One reason is that ice core samples may contain contaminants, e.g. traces of drill fluid, which can affect some parameters. Second, the mixing ratios for CH_4 , ethane and propane in Antarctic ice cores, especially from cold periods, are considerably lower than those in the working standards. Two different approaches were applied. (1) We measured horizontal ice core replicates, i.e. samples from exactly the same depth and therefore identical gas and impurity content. For this we used ice from the Antarctic shallow core B34 with the samples derived from two vertically neighbouring depth intervals (179.12 – 179.24 m and 179.24 – 179.36 m) with each interval providing four horizontal replicates. While most parameters show no difference between the two sections, air content and methyl chloride show differences (Tables 4 and 5). It is also notable that the ppt-level gas species for B34 show a higher variability when compared with TALDICE results, pointing to complex in situ production of these species in B34. (2) We

Table 6. Intercomparison of isotope measurements on N₂O of air cylinders between this study (Bern) and published data from CIC (Sperlich et al., 2013) and measurements performed at OSU (A. Schilt, personal communication, 2013). The differences (diff.) are calculated between Bern and the external results.

Cylinder name	$\delta^{15}\text{N-N}_2\text{O}$ (‰)			$\delta^{18}\text{O-N}_2\text{O}$ (‰)		
	Bern	CIC	diff.	Bern	CIC	diff.
NEEM*	6.97 ± 0.08	6.49 ± 0.04	0.48	43.52 ± 0.39	44.58 ± 0.06	-1.06
AL*	1.57 ± 0.47	1.01 ± 0.15	0.56	38.15 ± 0.39	38.80 ± 0.40	-0.65
NOAA*	-0.28 ± 0.18	-0.46 ± 0.15	0.18	40.25 ± 0.53	41.06 ± 0.40	-0.81
	Bern	OSU	diff.	Bern	OSU	diff.
Firn air NEEM FA32	9.16 ± 0.19	8.36 ± 0.12	0.80	44.91 ± 0.45	45.28 ± 0.29	-0.37

* Same names as used in Sperlich et al. (2013).

measured vertical replicates on the TALDICE core. In this case, samples are vertical neighbours, i.e. the enclosed air has a slightly different age. The age difference, Δa , of our neighbouring samples depends on the specific depth due to thinning of the ice in the ice sheet. For our neighbouring samples Δa is between 50 and 250 years. In view of the width of the age distribution of the enclosed air (about 40 and 70 years for Holocene and glacial conditions respectively, B. Bereiter, personal communication, 2013), these vertical replicates are rather independent atmospheric samples than identical replicates. Two different bin classes ($\Delta a < 80$ years and < 250 years) were selected to account for the different temporal variability of the parameters. From previous studies it is known that CH₄, a species with short atmospheric lifetime, shows high temporal variability, while e.g. $\delta^{15}\text{N-N}_2\text{O}$ varies more gradually allowing wider binning; thus more samples are regarded as replicates in this case. As expected, the reproducibility of most parameters is better for $\Delta a < 80$ years (Tables 4 and 5). For $\delta^{13}\text{C-CH}_4$, $\delta^{15}\text{N-N}_2\text{O}$ and $\delta^{18}\text{O-N}_2\text{O}$ the achieved reproducibility is better than in previous studies and also a step forward in terms of sample amount. In particular, in terms of N₂O isotope ratios previous studies used around twice or three times as much ice as used in our method. For the ppt-level gas methyl chloride, the ice core reproducibility is comparable to previous studies (Williams et al., 2007). Further, the precision for TALDICE samples is as good as for the firn air NEEM sample. Thus, the additional variability from the melting process is small (Table 5). This is important, as the methyl chloride blank contribution is about 20% of the measured ice core signal.

In the case of ethane and propane, results from other studies are only available for Greenland ice cores, with their much higher Northern Hemisphere background concentrations (Aydin et al., 2007). For our Antarctic samples, the reproducibility for ethane obtained on B34, WAIS and TALDICE ranges between 21 ppt for WAIS and 156 ppt for B34. More critical is that the reconstructed absolute mixing ratios exceed the modern values for Antarctica and those reconstructed from Antarctic firn air samples (Aydin et

al., 2011). Whole procedure blank measurements, “gas free ice as sample”, indicate that a large fraction of the ethane and propane signal of the Antarctic cores B34, WAIS and TALDICE is generated during the melting process from the vessel surfaces (Table 2). In contrast, for the samples from the Greenland NGRIP core, ethane (propane) values are factor 3 (4) larger than the blank, offering the possibility to explore these parameters further (Table 5). Methyl chloride values for these samples, however, are strongly elevated and point to ice in situ production or production during the melting of the sample (Table 5). As a conclusion for these ppt-species, the blank contribution is an issue for further analytical improvements; however, the non-atmospheric component generated by the ice itself is a more severe problem, limiting its usage in reliably reconstructing past mixing ratios.

5.4 Intercomparison

In the following we compare our results with measurements from other laboratories, as for most measured parameters there is not yet an official reference available. However, air and ice sample intercomparison round robins are currently underway. Given the large suite of parameters, not all measured species can be treated with the same detail here.

We focus on $\delta^{13}\text{C-CH}_4$, since several intercomparison samples have been measured by other groups as well, and only recently was an interference with Kr affecting several $\delta^{13}\text{C-CH}_4$ data sets identified (Schmitt et al., 2013). Ice samples from the Antarctic ice core B34 (our $\delta^{13}\text{C-CH}_4$ value: -47.10 ± 0.05 ‰) have also been measured previously by our colleagues at the Institute for Marine and Atmospheric Research Utrecht (IMAU) and at the Alfred Wegener Institute, Helmholtz Centre for Polar and Marine Research (AWI); Sapart et al. (2011) report $\delta^{13}\text{C-CH}_4$ values of -46.46 ± 0.21 ‰ for IMAU and -46.57 ± 0.13 ‰ for AWI. Both values were measured before the awareness of the Kr issue. According to Schmitt et al. (2013), the Kr correction would translate the IMAU and AWI numbers into lighter values, hence closer to our value. A second

ice core material allowing comparison with other groups is from the WAIS divide drill site (our WDCO5A core piece: bag 182, depth 170.99 m, ca. 1550 AD) provided by Todd Sowers from Penn State University (PSU). The Kr-corrected $\delta^{13}\text{C}\text{-CH}_4$ values from adjacent core sections from AWI is -47.81‰ (depth 166.78 m), -48.28‰ (depth 164.96 m) and -47.87‰ (depth 169.80 m) for two pieces measured at PSU (Möller et al., 2013), thus close to our value of -48.03‰ (Table 4). Further validation of the Kr-corrected data recently published by Möller et al. (2013) is provided by new measurements for the same time period using our new set-up and samples from the TALDICE core. The studied time interval shows a pronounced shift of 4‰ in $\delta^{13}\text{C}\text{-CH}_4$, thus ideal to capture the dynamic range of the methods as well (Fig. 9). The Kr-corrected results measured on EPICA Dronning Maud Land (EDML) and Vostok (Möller et al., 2013) fit well with our new data set from the TALDICE core taking the uncertainty of the age scales into account. Additionally, Fig. 9 allows for the comparison of the CH_4 mixing ratios obtained with different methods, all measured on the TALDICE core. Here, our $[\text{CH}_4]$ results agree well with those of Buiron et al. (2011) as well as with a high-resolution data set using the continuous-flow analysis system, with a precision of 15–20 ppb (Schüpbach et al., 2011). Finally, we compare results from a firn air sample (canister name “FA23”, depth 76 m, termed “firn air NEEM” in Tables 4 and 5) from the NEEM 2008 EU hole that has also been investigated by IMAU and the Centre for Ice and Climate, Copenhagen (CIC) (see Sapart et al., 2013). Our $\delta^{13}\text{C}\text{-CH}_4$ value of $-49.49 \pm 0.04\text{‰}$ agrees well with data from IMAU (Kr-corrected value, $-49.69 \pm 0.03\text{‰}$) and CIC (no Kr issue, $-49.52 \pm 0.13\text{‰}$).

As no official reference gas exists for the stable isotope ratios of N_2O , we tie our $\delta^{15}\text{N}\text{-N}_2\text{O}$ and $\delta^{18}\text{O}\text{-N}_2\text{O}$ values to those used at IMAU via urban air, “NAT332”. To assess the robustness of this single tie point NAT332, we compare results from three air samples that were provided and measured by CIC (Sperlich et al., 2013) and exchanged with our lab. For $\delta^{15}\text{N}\text{-N}_2\text{O}$, our values for all three cylinders are heavier than the CIC values, while our $\delta^{18}\text{O}\text{-N}_2\text{O}$ values are all lighter than CIC (Table 6). A second N_2O intercomparison using the “firn air NEEM” canister was conducted in collaboration with the laboratory at Oregon State University (OSU, Adrian Schilt). They tied their working standards for the N_2O isotope measurement to match the extrapolated values of the Cape Grim reconstruction (Park et al., 2012). For $\delta^{15}\text{N}\text{-N}_2\text{O}$ our value is again heavier by 0.8‰ compared to the OSU value and our $\delta^{18}\text{O}\text{-N}_2\text{O}$ is again slightly lighter than OSU (Table 6). Regarding the N_2O mixing ratios, the two methods agree well, with our value at $289 \pm 4\text{ ppb}$ and $291.2 \pm 1.1\text{ ppb}$ for OSU. In both intercomparison cases our $\delta^{15}\text{N}\text{-N}_2\text{O}$ values turned out to be heavier by 0.2 to 0.8‰ , whereas our $\delta^{18}\text{O}\text{-N}_2\text{O}$ values are lighter by 0.3 to 0.9‰ .

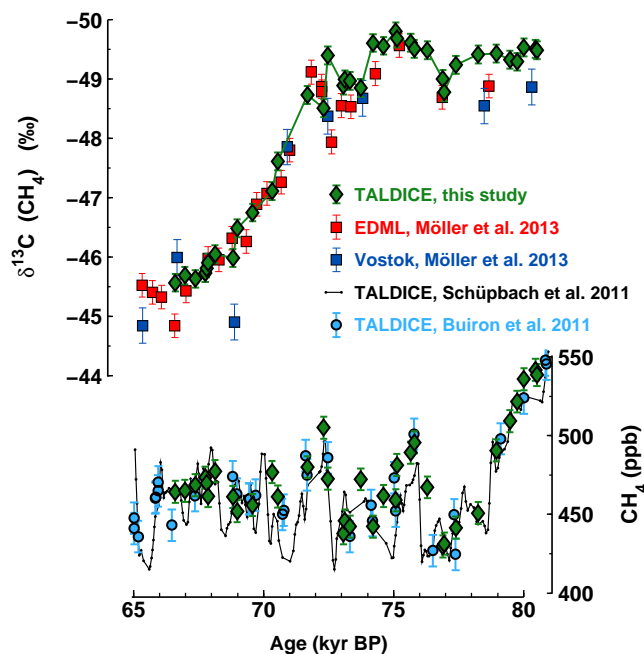


Figure 9. Comparison of our $\delta^{13}\text{C}\text{-CH}_4$ and $[\text{CH}_4]$ measurements with published results for an interval showing strong variations in both parameters. All data are plotted on a common age scale (Veres et al., 2013).

Similar to $\delta^{13}\text{C}\text{-CH}_4$, our WAIS divide intercomparison ice allows comparing with other groups’ results. Our methyl chloride value of $889 \pm 20\text{ ppt}$ is in accordance with measurements at University of Irvine (M. Aydin, personal communication, 2013) from neighbouring sections. A comparison of our TALDICE data from the Holocene with a recently published data set spanning the same period but measured on Taylor Dome ice (Verhulst et al., 2013) is complicated because the different variability in the two records may indicate in situ production.

6 Conclusions

We described a multi-parameter device to measure a large suite of trace gas species and their isotopic compositions on a single ice core sample and demonstrated its performance. The new system is based on an automated infrared melting device operated under vacuum, which allows for rapid extraction of the ice core air once released during the melting process. This principle combines high extraction efficiency with low helium consumption compared to techniques using a helium-purge set-up. A novel feature of our new device is the separation of drill fluid residues using a dedicated valve and backflush system.

With the help of our inhouse developed software routine, we are able to calculate $\delta^{13}\text{C}\text{-CH}_4$, and $\delta^{15}\text{N}\text{-N}_2\text{O}$, and $\delta^{18}\text{O}\text{-N}_2\text{O}$ values within a single acquisition run. To

prevent interference with Kr during the $\delta^{13}\text{C}$ - CH_4 measurement, Kr and CH_4 -derived CO_2 are separated. Improvement in precision was reached for $\delta^{15}\text{N}$ - N_2O and $\delta^{18}\text{O}$ - N_2O analyses, which now allows us to reconstruct the small variations hidden within measurement uncertainty in previous studies. Sample amount was reduced with respect to previous $\delta^{13}\text{C}$ - CH_4 and N_2O isotope studies.

To detect the other trace gas species (Xe, ethane, propane, methyl chloride, CCL_2F_2), we perform several peak jumps. Focusing the ion source to the m/z range of doubly charged Xe isotopes, we are the first to measure the isotopic composition on Xe^{2+} ions using GC-IRMS. The attained precision of 0.05 ‰ per mass unit allows us to correct the species' concentrations and isotopic ratios for gravitational effects in the firn column.

Acknowledgements. The Talos Dome Ice core project (TALDICE), a joint European programme, is funded by national contributions from Italy, France, Germany, Switzerland and the United Kingdom. Primary logistical support was provided by PNRA at Talos Dome. This is TALDICE publication no. 39. Financial support for this work has been provided in part by the European Research Council Advanced Grant MATRICs, and the Schweizerischer Nationalfonds (SNF project primeMETHANE). B34 ice core samples were provided by the Alfred Wegener Institute, Helmholtz Centre for Polar and Marine Research. We thank Matthias Baumgartner for measuring replicate ice core samples from the TALDICE core. Martin Vollmer from the Swiss Federal Laboratories for Materials Testing and Research (Empa) kindly calibrated our working standards for the ppt-level species. We thank Peter Nyfeler for calibrating our CO_2 cylinder. The authors are very grateful to Hinrich Schaefer and an anonymous reviewer for their thorough reviews and the many valuable suggestions on the discussion version which improved the final version of this manuscript.

Edited by: P. Herckes

References

- Abram, N. J., Mulvaney, R., Wolff, E., Triest, J., Kipfstuhl, S., Trusel, L. D., Vimeux, F., Fleet, L., and Arrowsmith, C.: Acceleration of snow melt in an Antarctic Peninsula ice core during the twentieth century, *Nat. Geosci.*, 6, 404–411, doi:10.1038/ngeo1787, 2013.
- Augustin, L., Panichi, S., and Frascati, F.: EPICA Dome C 2 drilling operations: performances, difficulties, results, *Ann. Glaciol.*, 47, 68–72, 2007.
- Aydin, M., De Bruyn, W. J., and Saltzman, E. S.: Preindustrial atmospheric carbonyl sulfide (OCS) from an Antarctic ice core, *Geophys. Res. Lett.*, 29, 1359, doi:10.1029/2002gl014796, 2002.
- Aydin, M., Williams, M. B., and Saltzman, E. S.: Feasibility of reconstructing paleoatmospheric records of selected alkanes, methyl halides, and sulfur gases from Greenland ice cores, *J. Geophys. Res. Atmos.*, 112, D07312, doi:10.1029/2006jd008027, 2007.
- Aydin, M., Montzka, S. A., Battle, M. O., Williams, M. B., De Bruyn, W. J., Butler, J. H., Verhulst, K. R., Tatum, C., Gun, B. K., Plotkin, D. A., Hall, B. D., and Saltzman, E. S.: Post-coring entrapment of modern air in some shallow ice cores collected near the firn-ice transition: evidence from CFC-12 measurements in Antarctic firn air and ice cores, *Atmos. Chem. Phys.*, 10, 5135–5144, doi:10.5194/acp-10-5135-2010, 2010.
- Aydin, M., Verhulst, K. R., Saltzman, E. S., Battle, M. O., Montzka, S. A., Blake, D. R., Tang, Q., and Prather, M. J.: Recent decreases in fossil-fuel emissions of ethane and methane derived from firn air, *Nature*, 476, 198–201, doi:10.1038/nature10352, 2011.
- Bazin, L., Landais, A., Lemieux-Dudon, B., Toyé Mahamadou Kele, H., Veres, D., Parrenin, F., Martinerie, P., Ritz, C., Capron, E., Lipenkov, V., Loutre, M.-F., Raynaud, D., Vinther, B., Svensson, A., Rasmussen, S. O., Severi, M., Blunier, T., Leuenberger, M., Fischer, H., Masson-Delmotte, V., Chappellaz, J., and Wolff, E.: An optimized multi-proxy, multi-site Antarctic ice and gas orbital chronology (AICC2012): 120–800 ka, *Clim. Past*, 9, 1715–1731, doi:10.5194/cp-9-1715-2013, 2013.
- Behrens, M., Schmitt, J., Richter, K.-U., Bock, M., Richter, U., Levin, I., and Fischer, H.: A gas chromatography/combustion/isotope ratio mass spectrometry system for high-precision $\delta^{13}\text{C}$ measurements of atmospheric methane extracted from ice core samples, *Rapid. Commun. Mass Spectrom.*, 22, 3261–3269, doi:10.1002/rcm.3720, 2008.
- Bock, M., Schmitt, J., Behrens, M., Möller, L., Schneider, R., Sapart, C., and Fischer, H.: A gas chromatography/pyrolysis/isotope ratio mass spectrometry system for high-precision δD measurements of atmospheric methane extracted from ice cores, *Rapid. Commun. Mass Spectrom.*, 24, 621–633, doi:10.1002/rcm.4429, 2010a.
- Bock, M., Schmitt, J., Möller, L., Spahni, R., Blunier, T., and Fischer, H.: Hydrogen Isotopes Preclude Marine Hydrate CH_4 Emissions at the Onset of Dansgaard-Oeschger Events, *Science*, 328, 1686–1689, doi:10.1126/science.1187651, 2010b.
- Bock, M., Schmitt, J., Beck, J., Schneider, R., and Fischer, H.: Improving accuracy and precision of ice core $\delta\text{D}(\text{CH}_4)$ analyses using methane pre-pyrolysis and hydrogen post-pyrolysis trapping and subsequent chromatographic separation, *Atmos. Meas. Tech.*, 7, 1999–2012, doi:10.5194/amt-7-1999-2014, 2014.
- Buiron, D., Chappellaz, J., Stenni, B., Frezzotti, M., Baumgartner, M., Capron, E., Landais, A., Lemieux-Dudon, B., Masson-Delmotte, V., Montagnat, M., Parrenin, F., and Schilt, A.: TALDICE-1 age scale of the Talos Dome deep ice core, East Antarctica, *Clim. Past*, 7, 1–16, doi:10.5194/cp-7-1-2011, 2011.
- Craig, H., Horibe, Y., and Sowers, T.: Gravitational separation of gases and isotopes in polar ice caps, *Science*, 242, 1675–1678, 1988.
- Faïn, X., Chappellaz, J., Rhodes, R. H., Stowasser, C., Blunier, T., McConnell, J. R., Brook, E. J., Preunkert, S., Legrand, M., Debois, T., and Romanini, D.: High resolution measurements of carbon monoxide along a late Holocene Greenland ice core: evidence for in situ production, *Clim. Past*, 10, 987–1000, doi:10.5194/cp-10-987-2014, 2014.
- Ferretti, D. F., Miller, J. B., White, J. W. C., Etheridge, D. M., Lassey, K. R., Lowe, D. C., Meure, C. M. M., Dreier, M. F., Trudinger, C. M., van Ommen, T. D., and Langenfelds, R. L.: Unexpected changes to the global methane budget over the past 2000 years, *Science*, 309, 1714–1717, doi:10.1126/science.1115193, 2005.

- Flückiger, J., Blunier, T., Stauffer, B., Chappellaz, J., Spahni, R., Kawamura, K., Schwander, J., Stocker, T. F., and DahlJensen, D.: N₂O and CH₄ variations during the last glacial epoch: Insight into global processes, *Global Biogeochem Cy*, 18, GB1020, doi:10.1029/2003gb002122, 2004.
- Headly, M. A.: Krypton and xenon in air trapped in polar ice cores: Paleo-atmospheric measurements for estimating past mean ocean temperature and summer snowmelt frequency, PhD dissertation, University of California San Diego, 229 pp., 2008.
- Headly, M. A. and Severinghaus, J. P.: A method to measure Kr/N₂ ratios in air bubbles trapped in ice cores and its application in reconstructing past mean ocean temperature, *J. Geophys. Res.*, 112, D19105, doi:10.1029/2006JD008317, 2007.
- Hörhold, M. W., Laepple, T., Freitag, J., Bigler, M., Fischer, H., and Kipfstuhl, S.: On the impact of impurities on the densification of polar firn, *Earth Planet Sc. Lett.*, 325, 93–99, doi:10.1016/j.epsl.2011.12.022, 2012.
- Kaspers, K. A., van de Wal, R. S. W., de Gouw, J. A., Hofstede, C. M., van den Broeke, M. R., van der Veen, C., Neubert, R. E. M., Meijer, H. A. J., Brenninkmeijer, C. A. M., Karlof, L., and Winther, J. G.: Analyses of firn gas samples from Dronning Maud Land, Antarctica: Study of nonmethane hydrocarbons and methyl chloride, *J. Geophys. Res. Atmos.*, 109, D02307, doi:10.1029/2003jd003950, 2004.
- Kawamura, K., Nakazawa, T., Aoki, S., Sugawara, S., Fujii, Y., and Watanabe, O.: Atmospheric CO₂ variations over the last three glacial-interglacial climatic cycles deduced from the Dome Fuji deep ice core, Antarctica using a wet extraction technique, *Tellus Ser. B*, 55, 126–137, doi:10.1034/j.1600-0889.2003.00050.x, 2003.
- Kawamura, K., Severinghaus, J. P., Albert, M. R., Courville, Z. R., Fahnestock, M. A., Scambos, T., Shields, E., and Shuman, C. A.: Kinetic fractionation of gases by deep air convection in polar firn, *Atmos. Chem. Phys.*, 13, 11141–11155, doi:10.5194/acp-13-11141-2013, 2013.
- Landais, A., Barnola, J. M., Kawamura, K., Caillon, N., Delmotte, M., Van Ommen, T., Dreyfus, G., Jouzel, J., Masson-Delmotte, V., and Minster, B.: Firn-air $\delta^{15}\text{N}$ in modern polar sites and glacial-interglacial ice: a model-data mismatch during glacial periods in Antarctica?, *Quaternary Sci. Rev.*, 25, 49–62, doi:10.1016/j.quascirev.2005.06.007, 2006.
- Lipenkov, V., Candaudap, F., Ravoire, J., Dulac, E., and Raynaud, D.: A new device for the measurement of air content in polar ice, *J. Glaciol.*, 41, 423–429, 1995.
- Loulergue, L., Schilt, A., Spahni, R., Masson-Delmotte, V., Blunier, T., Lemieux, B., Barnola, J.-M., Raynaud, D., Stocker, T. F., and Chappellaz, J.: Orbital and millennial-scale features of atmospheric CH₄ over the past 800,000 years, *Nature*, 453, 383–386, doi:10.1038/nature06950, 2008.
- Lüthi, D., Le Floch, M., Bereiter, B., Blunier, T., Barnola, J. M., Siegenthaler, U., Raynaud, D., Jouzel, J., Fischer, H., Kawamura, K., and Stocker, T. F.: High-resolution carbon dioxide concentration record 650 000–800 000 years before present, *Nature*, 453, 379–382, doi:10.1038/nature06949, 2008.
- Melton, J. R., Whiticar, M. J., and Eby, P.: Stable carbon isotope ratio analyses on trace methane from ice samples, *Chemical Geology*, 288, 88–96, doi:10.1016/j.chemgeo.2011.03.003, 2011.
- Möller, L., Sowers, T., Bock, M., Spahni, R., Behrens, M., Schmitt, J., Miller, H., and Fischer, H.: Independent variations of CH₄ emissions and isotopic composition over the past 160,000 years, *Nat. Geosci.*, 6, 885–890, doi:10.1038/ngeo1922, 2013.
- NEEM community members: Eemian interglacial reconstructed from a Greenland folded ice core, *Nature*, 493, 489–494, doi:10.1038/nature11789, 2013.
- Park, S., Croteau, P., Boering, K. A., Etheridge, D. M., Ferretti, D., Fraser, P. J., Kim, K. R., Krummel, P. B., Langenfelds, R. L., van Ommen, T. D., Steele, L. P., and Trudinger, C. M.: Trends and seasonal cycles in the isotopic composition of nitrous oxide since 1940, *Nat. Geosci.*, 5, 261–265, doi:10.1038/ngeo1421, 2012.
- Pozzer, A., Pollmann, J., Taraborrelli, D., Jöckel, P., Helmig, D., Tans, P., Hueber, J., and Lelieveld, J.: Observed and simulated global distribution and budget of atmospheric C₂–C₅ alkanes, *Atmos. Chem. Phys.*, 10, 4403–4422, doi:10.5194/acp-10-4403-2010, 2010.
- Rahn, T. and Wahlen, M.: A reassessment of the global isotopic budget of atmospheric nitrous oxide, *Global Biogeochem. Cy.*, 14, 537–543, doi:10.1029/1999gb900070, 2000.
- Raynaud, D. and Lebel, B.: Total gas content and surface elevation of polar ice sheets, *Nature*, 281, 289–291, doi:10.1038/281289a0, 1979.
- Raynaud, D., Lipenkov, V., Lemieux-Dudon, B., Duval, P., Loutre, M.-F., and Lhomme, N.: The local insolation signature of air content in Antarctic ice. A new step toward an absolute dating of ice records, *Earth Planet Sc. Lett.*, 261, 337–349, doi:10.1016/j.epsl.2007.06.025, 2007.
- Rhodes, R. H., Fain, X., Stowasser, C., Blunier, T., Chappellaz, J., McConnell, J. R., Romanini, D., Mitchell, L. E., and Brook, E. J.: Continuous methane measurements from a late Holocene Greenland ice core: Atmospheric and in-situ signals, *Earth Planet Sc. Lett.*, 368, 9–19, doi:10.1016/j.epsl.2013.02.034, 2013.
- Ritz, S. P., Stocker, T. F., and Severinghaus, J. P.: Noble gases as proxies of mean ocean temperature: sensitivity studies using a climate model of reduced complexity, *Quat. Sci. Rev.*, 30, 3728–3741, doi:10.1016/j.quascirev.2011.09.021, 2011.
- Rubino, M., Etheridge, D. M., Trudinger, C. M., Allison, C. E., Battle, M. O., Langenfelds, R. L., Steele, L. P., Curran, M., Bender, M., White, J. W. C., Jenk, T. M., Blunier, T., and Francey, R. J.: A revised 1000-year atmospheric $\delta^{13}\text{C-CO}_2$ record from Law Dome and South Pole, Antarctica, *J. Geophys. Res. Atmos.*, 118, 8482–8499, doi:10.1002/jgrd.50668, 2013.
- Saito, T., Yokouchi, Y., Aoki, S., Nakazawa, T., Fujii, Y., and Watanabe, O.: A method for determination of methyl chloride concentration in air trapped in ice cores, *Chemosphere*, 63, 1209–1213, doi:10.1016/j.chemosphere.2005.08.075, 2006.
- Saltzman, E. S., Aydin, M., Williams, M. B., Verhulst, K. R., and Gun, B.: Methyl chloride in a deep ice core from Siple Dome, Antarctica, *Geophys. Res. Lett.*, 36, L03822, doi:10.1029/2008gl036266, 2009.
- Sapart, C. J., van der Veen, C., Vigano, I., Brass, M., van de Wal, R. S. W., Bock, M., Fischer, H., Sowers, T., Buizert, C., Sperlich, P., Blunier, T., Behrens, M., Schmitt, J., Seth, B., and Röckmann, T.: Simultaneous stable isotope analysis of methane and nitrous oxide on ice core samples, *Atmos. Meas. Tech.*, 4, 2607–2618, doi:10.5194/amt-4-2607-2011, 2011.
- Sapart, C. J., Martinerie, P., Witrant, E., Chappellaz, J., van de Wal, R. S. W., Sperlich, P., van der Veen, C., Bernard, S., Sturges, W. T., Blunier, T., Schwander, J., Etheridge, D., and Röckmann, T.: Can the carbon isotopic composition of methane be reconstructed

- from multi-site firn air measurements?, *Atmos. Chem. Phys.*, 13, 6993–7005, doi:10.5194/acp-13-6993-2013, 2013.
- Schaefer, H. and Whiticar, M. J.: Measurement of stable carbon isotope ratios of methane in ice samples, *Organic Geochemistry*, 38, 216–226, doi:10.1016/j.orggeochem.2006.10.006, 2007.
- Schilt, A., Baumgartner, M., Schwander, J., Buiron, D., Capron, E., Chappellaz, J., Loulergue, L., Schüpbach, S., Spahni, R., Fischer, H., and Stocker, T. F.: Atmospheric nitrous oxide during the last 140,000 years, *Earth Planet. Sc. Lett.*, 300, 33–43, doi:10.1016/j.epsl.2010.09.027, 2010.
- Schmitt, J.: A sublimation technique for high-precision $\delta^{13}\text{C}$ on CO_2 and CO_2 mixing ratio from air trapped in deep ice cores, University of Bremen, 2006.
- Schmitt, J., Schneider, R., and Fischer, H.: A sublimation technique for high-precision measurements of $\delta^{13}\text{CO}_2$ and mixing ratios of CO_2 and N_2O from air trapped in ice cores, *Atmos. Meas. Tech.*, 4, 1445–1461, doi:10.5194/amt-4-1445-2011, 2011.
- Schmitt, J., Schneider, R., Elsig, J., Leuenberger, D., Lourantou, A., Chappellaz, J., Köhler, P., Joos, F., Stocker, T. F., Leuenberger, M., and Fischer, H.: Carbon isotope constraints on the deglacial CO_2 rise from ice cores, *Science*, 336, 711–714, doi:10.1126/science.1217161, 2012.
- Schmitt, J., Seth, B., Bock, M., van der Veen, C., Möller, L., Sapart, C. J., Prokopiou, M., Sowers, T., Röckmann, T., and Fischer, H.: On the interference of Kr during carbon isotope analysis of methane using continuous-flow combustion-isotope ratio mass spectrometry, *Atmos. Meas. Tech.*, 6, 1425–1445, doi:10.5194/amt-6-1425-2013, 2013.
- Schüpbach, S., Federer, U., Bigler, M., Fischer, H., and Stocker, T. F.: A refined TALDICE-1a age scale from 55 to 112 ka before present for the Talos Dome ice core based on high-resolution methane measurements, *Clim. Past*, 7, 1001–1009, doi:10.5194/cp-7-1001-2011, 2011.
- Severinghaus, J. P., Grachev, A., and Battle, M.: Thermal fractionation of air in polar firn by seasonal temperature gradients, *G-Cubed*, 2, 146, doi:10.1029/2000GC000146, 2001.
- Sowers, T., Alley, R. B., and Jubenville, J.: Ice core records of atmospheric N_2O covering the last 106,000 years, *Science*, 301, 945–948, doi:10.1126/science.1085293, 2003.
- Sowers, T., Bernard, S., Aballain, O., Chappellaz, J., Barnola, J. M., and Marik, T.: Records of the $\delta^{13}\text{C}$ of atmospheric CH_4 over the last 2 centuries as recorded in Antarctic snow and ice, *Global Biogeochem. Cy.*, 19, GB2002, doi:10.1029/2004GB002408, 2005.
- Sperlich, P., Buizert, C., Jenk, T. M., Sapart, C. J., Prokopiou, M., Röckmann, T., and Blunier, T.: An automated GC-C-GC-IRMS setup to measure palaeoatmospheric $\delta^{13}\text{C-CH}_4$, $\delta^{15}\text{N-N}_2\text{O}$ and $\delta^{18}\text{O-N}_2\text{O}$ in one ice core sample, *Atmos. Meas. Tech.*, 6, 2027–2041, doi:10.5194/amt-6-2027-2013, 2013.
- Tschumi, J. and Stauffer, B.: Reconstructing past atmospheric CO_2 concentration based on ice-core analyses: open questions due to in situ production of CO_2 in the ice, *J. Glaciol.*, 46, 45–53, 2000.
- Veres, D., Bazin, L., Landais, A., Toyé Mahamadou Kele, H., Lemieux-Dudon, B., Parrenin, F., Martinerie, P., Blayo, E., Blunier, T., Capron, E., Chappellaz, J., Rasmussen, S. O., Severi, M., Svensson, A., Vinther, B., and Wolff, E. W.: The Antarctic ice core chronology (AICC2012): an optimized multi-parameter and multi-site dating approach for the last 120 thousand years, *Clim. Past*, 9, 1733–1748, doi:10.5194/cp-9-1733-2013, 2013.
- Verhulst, K. R., Aydin, M., and Saltzman, E. S.: Methyl chloride variability in the Taylor Dome ice core during the Holocene, *J. Geophys. Res. Atmos.*, 118, 1–11, doi:10.1002/2013JD020197, 2013.
- Vigano, I., Röckmann, T., Holzinger, R., van Dijk, A., Keppler, F., Greule, M., Brand, W. A., Geilmann, H., and van Weelden, H.: The stable isotope signature of methane emitted from plant material under UV irradiation, *Atmos. Environ.*, 43, 5637–5646, doi:10.1016/j.atmosenv.2009.07.046, 2009.
- Wang, Z., Chappellaz, J., Park, K., and Mak, J. E.: Large Variations in Southern Hemisphere Biomass Burning During the Last 650 Years, *Science*, 330, 1663–1666, doi:10.1126/science.1197257, 2010.
- Weiss, R. F.: The solubility of nitrogen, oxygen and argon in water and seawater, *Deep-Sea Res.*, 17, 721–735, doi:10.1016/0011-7471(70)90037-9, 1970.
- Werner, R. A. and Brand, W. A.: Referencing strategies and techniques in stable isotope ratio analysis, *Rapid. Commun. Mass Spectrom.*, 15, 501–519, doi:10.1002/rcm.258, 2001.
- Whiticar, M. and Schaefer, H.: Constraining past global tropospheric methane budgets with carbon and hydrogen isotope ratios in ice, *Phil. Trans. R. Soc. A*, 365, 1793–1828, doi:10.1098/rsta.2007.2048, 2007.
- Williams, M. B., Aydin, M., Tatum, C., and Saltzman, E. S.: A 2000 year atmospheric history of methyl chloride from a South Pole ice core: Evidence for climate-controlled variability, *Geophys. Res. Lett.*, 34, L07811, doi:10.1029/2006gl029142, 2007.
- Worton, D. R., Sturges, W. T., Reeves, C. E., Newland, M. J., Penkett, S. A., Atlas, E., Stroud, V., Johnson, K., Schmidbauer, N., Solberg, S., Schwander, J., and Barnola, J.-M.: Evidence from firn air for recent decreases in non-methane hydrocarbons and a 20th century increase in nitrogen oxides in the northern hemisphere, *Atmos. Environ.*, 54, 592–602, doi:10.1016/j.atmosenv.2012.02.084, 2012.
- Xiao, X., Prinn, R. G., Fraser, P. J., Simmonds, P. G., Weiss, R. F., O'Doherty, S., Miller, B. R., Salameh, P. K., Harth, C. M., Krummel, P. B., Porter, L. W., Mühle, J., Grealley, B. R., Cunnold, D., Wang, R., Montzka, S. A., Elkins, J. W., Dutton, G. S., Thompson, T. M., Butler, J. H., Hall, B. D., Reimann, S., Vollmer, M. K., Stordal, F., Lunder, C., Maione, M., Arduini, J., and Yokouchi, Y.: Optimal estimation of the surface fluxes of methyl chloride using a 3-D global chemical transport model, *Atmos. Chem. Phys.*, 10, 5515–5533, doi:10.5194/acp-10-5515-2010, 2010.